Three-dimensional structure and evolution of stratospheric HNO_3 based on UARS Microwave Limb Sounder measurements

M. L. Santee
Jet Propulsion Laboratory, California Institute of Technology, Pasadena, California, USA

G. L. Manney
Jet Propulsion Laboratory, California Institute of Technology, Pasadena, California, USA

Department of Natural Sciences, New Mexico Highlands University, Las Vegas, New Mexico, USA

N. J. Livesey and W. G. Read
Jet Propulsion Laboratory, California Institute of Technology, Pasadena, California, USA

Received 27 January 2004; revised 14 April 2004; accepted 24 May 2004; published 7 August 2004.

[1] The Upper Atmosphere Research Satellite (UARS) Microwave Limb Sounder (MLS) measured the global distribution of stratospheric HNO_3 through more than seven complete annual cycles in both hemispheres. Here we present an overview of the seasonal, interhemispheric, and interannual variations in the distribution of HNO_3 throughout the lower and middle stratosphere from 420 to 960 K potential temperature based on the UARS MLS version 6 HNO_3 measurements. The version 6 MLS data have much better precision and a larger vertical range than previous MLS HNO_3 data sets and have also been corrected to account for an oversight in the retrieval algorithms that led earlier versions to overestimate HNO_3 abundances by as much as 35% at some levels in the stratosphere. HNO_3 exhibits little vertical, seasonal, or interannual variability in the tropics. For the first $\sim$1.5 years of the mission, however, a persistent enhancement is seen at low and middle latitudes that we attribute to perturbations in reactive nitrogen chemistry under conditions of high aerosol loading from the eruption of Mount Pinatubo. The signature of Pinatubo-induced HNO_3 enhancement is considerably weaker at 420 and 465 K than it is at higher altitudes, and it is also considerably weaker at northern middle and high latitudes than it is in the Southern Hemisphere. HNO_3 abundances increase toward the pole in both hemispheres at all levels and in all seasons, with the exception of the severely denitrified region inside the Antarctic vortex. A pronounced seasonal cycle is present at middle and high latitudes up to at least 960 K ($\sim$34 km), with a winter maximum and a summer minimum. Large interannual variability in the timing, magnitude, and duration of enhanced wintertime HNO_3 abundances is seen in both hemispheres. Even in the coldest Arctic winters, HNO_3 depletion is modest and limited in both horizontal and vertical extent. In contrast, virtually complete removal of gas-phase HNO_3 occurs at the highest southern latitudes by July in every year throughout the lower stratosphere. Indications of denitrification are present up to at least 740 K, well above the highest altitude at which dehydration is observed, providing further evidence that denitrification can proceed in the absence of dehydration. *INDEX TERMS:* 0340 Atmospheric Composition and Structure: Middle atmosphere—composition and chemistry; 0341 Atmospheric Composition and Structure: Middle atmosphere—constituent transport and chemistry (3334); 0394 Atmospheric Composition and Structure: Instruments and techniques; *KEYWORDS:* Microwave Limb Sounder (MLS), Upper Atmosphere Research Satellite (UARS), nitric acid (HNO_3), denitrification, polar processes, stratospheric chemistry

Citation: Santee, M. L., G. L. Manney, N. J. Livesey, and W. G. Read (2004), Three-dimensional structure and evolution of stratospheric HNO_3 based on UARS Microwave Limb Sounder measurements, *J. Geophys. Res.*, *109*, D15306, doi:10.1029/2004JD004578.

0148-0227/04/2004JD004578$09.00

1. Introduction

[2] Nitric acid (HNO_3) plays several pivotal roles in the processes controlling stratospheric ozone depletion [e.g., *Solomon*, 1999; *World Meteorological Organization*,

2003]. Over the past few decades, HNO_3 has been measured by a variety of ground-based, aircraft, balloon, and satellite instruments [see *Santee et al.*, 1999, and references therein]. By far the most complete observational record has been obtained by the Microwave Limb Sounder (MLS) on board the Upper Atmosphere Research Satellite (UARS), which measured the global distribution of stratospheric HNO_3 over annual cycles for much of the 1990s, albeit with reduced sampling frequency in the latter half of the decade. The unparalleled scope of the UARS MLS HNO_3 data set is underscored in Table 1, in which it is compared to the other spaced-based HNO_3 measurements available to date. The UARS MLS HNO_3 data set was previously examined by *Santee et al.* [1999] to explore the seasonal, interhemispheric, and interannual variations in the distribution of HNO_3. Although important conclusions were drawn from that study, it suffered from a number of limitations: It was confined to a single potential temperature level in the lower stratosphere (465 K, ~19-km altitude), it was based on version 4 MLS data, and it relied heavily on zonal-mean comparisons of the evolution of HNO_3 in the Northern and Southern Hemispheres. Here we update and significantly expand the previous work by examining the distribution of HNO_3 throughout the lower and middle stratosphere from 420 to 960 K. We use version 6 MLS HNO_3 data, which, in addition to having much better precision, a larger vertical range, and better definition of the HNO_3 profile, have also been corrected to account for the neglect of some excited vibrational state lines that caused the version 4 (and version 5) retrievals to substantially overestimate HNO_3 peak values [*Livesey et al.*, 2003]. In addition, we calculate averages over equivalent latitude (the latitude that would enclose the same area between it and the pole as a given contour of potential vorticity [*Butchart and Remsberg*, 1986]); such averages give a much more representative view of the behavior of HNO_3 in the context of the stratospheric flow and vortex evolution than zonal means, especially in the Arctic winter.

[3] In section 2 we briefly review the UARS MLS data coverage and summarize the quality of the version 6 HNO_3 measurements. We then examine time series of different slices through the data to develop a comprehensive picture of the mean evolution of stratospheric HNO_3 during the UARS time frame. Seasonal ''snapshots'' (maps and equivalent latitude/potential temperature cross sections) are shown to illustrate the typical behavior of HNO_3 during several intervals of particular interest in the annual cycle. Composite fields are derived by averaging together the results for individual years. This composite data set, which can be considered a climatology over substantial portions of the globe as discussed below, provides a valuable baseline for comparison with observations expected from NASA's upcoming Earth Observing System (EOS) Aura mission. Aura will carry several instruments capable of measuring HNO_3 in the stratosphere, including a second-generation MLS experiment. The improvements over UARS anticipated in the EOS MLS HNO_3 measurements are discussed in section 5.

2. MLS HNO_3 Data Coverage and Quality

[4] Microwave limb sounding and the UARS MLS instrument are described by, for example, *Waters* [1993], *Barath et al.* [1993], and *Waters et al.* [1999]. Latitudinal coverage of the MLS measurements extended from ~80° on one side of the equator to ~34° on the other. Approximately 10 times per year, UARS performed a 180° yaw maneuver such that MLS alternated between viewing northern and southern high latitudes, with the first day of a given UARS yaw period occurring ~5 days earlier each year. As a consequence, on a particular day of the year, MLS may have been viewing northern high latitudes in some years but southern high latitudes in others. A calendar of MLS daily data coverage and a detailed chronology of MLS operations are provided by *Livesey et al.* [2003] (see also section 2.1 of *Santee et al.* [1999]). After several years in orbit, degradation in the performance of the MLS antenna scan mechanism, together with a reduction in power available from the UARS spacecraft, resulted in markedly reduced data sampling. The relative sparsity of the data collected after 1998 limits their utility in establishing a climatology of this kind, and they are not included here.

[5] A full description of the MLS version 5 (v5) retrieval algorithms and resulting data set is given by *Livesey et al.* [2003]. Here we very briefly describe the major changes in the algorithms and their impact on the HNO_3 retrievals. The most significant change is that in v5, geophysical parameters are retrieved on every UARS surface (six surfaces per decade change in pressure, as opposed to three in previous MLS data sets). The v5 retrievals thus allow better definition of the HNO_3 profile. The inherent vertical resolution of the instrument is coarser than the v5 retrieval grid, however. Furthermore, vertical smoothing is applied to enhance retrieval stability. As a consequence, the true vertical resolution of the v5 HNO_3 data (which varies with altitude from 4.5 km at 100 hPa to 10.5 km at 4.6 hPa) is approximately the same as, and the v5 profiles are generally smoother than, in version 4 (v4). Along with the smoothing, more rigorous error propagation as well as improvements in the ozone (retrieved in the same band as HNO_3) and tangent pressure retrievals have led to substantially better (by a factor of 2–3) HNO_3 precision in v5 than in v4, even though the v5 retrievals are performed on every UARS surface; the single-profile precision is now ~1.0–1.5 ppbv throughout the vertical range. In addition, inclusion in the retrievals of the emission from several weak HNO_3 lines in the bands primarily used to measure ClO has provided information at higher altitudes and has extended the vertical range for reliable measurements up to 4.6 hPa (from 22 hPa in v4). Finally, strong negative biases (2–3 ppbv over a broad area) in the equatorial regions at 22 and 46 hPa present in the v4 HNO_3 data have been eliminated in this version.

[6] After the MLS v5 data reprocessing was completed, it was discovered that neglecting emission from HNO_3 ν_9 and ν_7 excited vibrational states caused v5 (and v4) values to significantly overestimate HNO_3 abundances at some levels in the stratosphere. An empirical correction to the MLS v5 HNO_3 data set has been derived and is described in detail by *Livesey et al.* [2003]. The correction is a linear, strongly temperature-dependent scaling that leads to reductions in the reported v5 HNO_3 mixing ratios of about 4–8% at 100 hPa, 10–20% at 32 hPa, and 25–35% at 10 hPa, depending on the latitude and season. The corrected MLS HNO_3 data set is referred to as ''v6.'' The v6 HNO_3 data are

Table 1. Space-Based HNO_3 Measurements

Instrument Name	Dates of Operation	Geographical Coverage	Horizontal Resolution,[a] km	Vertical Resolution, km	Accuracy/Precision[b]
UARS MLS[c]	19 Sept. 1991 to 29 March 2000	80°S to 80°N[d]	~400	5–10	~3 ppbv, 1.0–1.5 ppbv
LIMS[e]	25 Oct. 1978 to 28 May 1979	64°S to 84°N	~300	~2	~20%, ~0.1 ppbv
ATMOS/Spacelab-3[f]	30 April to 1 May 1985	29°–33°N, 47°–49°S	200–250	~4	16%, 10%
CIRRIS-1A[g]	29 April 1991	~36°S, ~65°N	~350	~3	~25%
ISAMS[h]	26 Sept. 1991 to 29 July 1992	80°S to 80°N	~400	~2.5	NA
CLAES[i]	25 Oct. 1991 to 25 April 1993	80°S to 80°N[d]	~400	~3	~15%, ~1 ppbv
ATMOS/ATLAS-1[j]	25 March to 2 April 1992	56°–22°S, 28°S–30°N	200–250	2–3	16%, 10%
ATMOS/ATLAS-2[j]	8–16 April 1993	50°–27°S, 64°–69°N	200–250	2–3	16%, 10%
ATMOS/ATLAS-3[j]	3–12 Nov. 1994	72°–64°S, 3°–49°N	200–250	2–3	16%, 10%
CRISTA[k]	4–12 Nov. 1994	57°S to 67°N	~200	2–3	12–30%, 3–5%
ILAS[l]	30 Oct. 1996 to 29 June 1997	64°–88°S, 57°–71°N[m]	220–230	1.9–3.5	<3%, <17%
Odin/SMR[n]	Nov. 2001 to present	83°S to 83°N	~500	~2	~20%
ENVISAT MIPAS[o]	March 2002 to present	90°S to 90°N	~500	~3	~10%, ~5%
ILAS-II[p]	2 April to 24 Oct. 2003	65°–88°S, 54–71°N[m]	220–230	1.3–2.9	NA
ACE-FTS[q]	Jan. 2004 to present	90°S to 90°N[m]	~300	3–4	NA

[a]Refers to the horizontal footprint of one profile, rather than the spacing between profiles.
[b]Single-profile values. In some cases, separate accuracy and precision estimates were not provided; in cases where error estimates were given as a function of altitude, the values listed here pertain to the lower stratosphere.
[c]Upper Atmosphere Research Satellite Microwave Limb Sounder; note that the data sampling frequency was significantly reduced after 1994.
[d]High-latitude coverage was discontinuous because of the UARS yaw maneuvers; see section 2.
[e]Limb Infrared Monitor of the Stratosphere [*Gille and Russell*, 1984; *Gille et al.*, 1984].
[f]Atmospheric Trace Molecule Spectroscopy experiment [*Russell et al.*, 1988; *Irion et al.*, 2002; F. W. Irion, personal communication, 2004].
[g]Cryogenic Infrared Radiance Instrumentation for Shuttle [*Bingham et al.*, 1997].
[h]Improved Stratospheric and Mesospheric Sounder [*Taylor et al.*, 1994, 1995]; accuracy and precision information are not available for the ISAMS HNO_3 measurements.
[i]Cryogenic Limb Array Etalon Spectrometer [*Kumer et al.*, 1996; *Danilin et al.*, 2000].
[j]Atmospheric Trace Molecule Spectroscopy experiment on the Atmospheric Laboratory for Applications and Science missions [*Gunson et al.*, 1996; *Irion et al.*, 2002; F. W. Irion, personal communication, 2004].
[k]Cryogenic Infrared Spectrometers and Telescopes for the Atmosphere [*Offermann et al.*, 1999; *Riese et al.*, 1999].
[l]Improved Limb Atmospheric Spectrometer [*Koike et al.*, 2000; *Irie et al.*, 2002; H. Irie, personal communication, 2004].
[m]The latitude coverage of this solar occultation instrument has strong temporal variation over this range.
[n]SubMillimetre Radiometer [P. Ricaud, personal communication, 2004; *Murtagh et al.*, 2002].
[o]Environmental Satellite Michelson Interferometer for Passive Atmospheric Sounding [H. Oelhaf, personal communication, 2004; *Fischer and Oelhaf*, 1996].
[p]Improved Limb Atmospheric Spectrometer II (H. Irie, personal communication, 2004); information about accuracy and precision is not yet available for the ILAS-II HNO_3 measurements.
[q]Atmospheric Chemistry Experiment–Fourier Transform Spectrometer (C. Randall, personal communication, 2004); information about accuracy and precision is not yet available for the ACE-FTS HNO_3 measurements.

available from the NASA Goddard Space Flight Center Distributed Active Archive Center (GSFC DAAC).

[7] *Livesey et al.* [2003] summarize comparisons of MLS v6 HNO_3 with other HNO_3 data sets, including those from the UARS Cryogenic Limb Array Etalon Spectrometer (CLAES), the Atmospheric Trace Molecule Spectroscopy (ATMOS) experiment, the Improved Limb Atmospheric Spectrometer (ILAS) [see also *Danilin et al.*, 2002], and the Ground-based Millimeter-wave Spectrometer (GBMS) [see also *Muscari et al.*, 2002]. Although comparisons between MLS and these other instruments do not always provide a consistent picture, they suggest that the following artifacts are present in the MLS v6 HNO_3 data: (1) a high bias of as much as ~2–3 ppbv in the equatorial regions during the first ~100 days of the mission, caused by enhanced stratospheric SO_2 (which is not retrieved as part of the v5 data processing) from the eruption of Mount Pinatubo, (2) a high bias of as much as 3–5 ppbv during Antarctic late winter at 585 and 620 K (with a smaller effect at 520 K), arising from nonlinearities with respect to temperature in the MLS retrieval system, and (3) a low bias of ~1–3 ppbv at the topmost levels (above 740 K, ~10–15 hPa). On the basis of the comparisons reported by *Livesey et al.* [2003], the MLS v6 HNO_3 data are expected to be accurate to within ~3 ppbv above ~15 hPa and ~2 ppbv below, except in the lower stratospheric winter polar vortices, where biases may be slightly larger.

3. HNO_3 Climatology From UARS MLS

3.1. Equivalent Latitude Time Series

[8] We begin by showing a time series to track the mean evolution of stratospheric HNO_3 over seven annual cycles in both hemispheres. The averages shown in Figure 1 are similar to zonal means, but they have been calculated as a function of potential vorticity (PV) expressed in terms of equivalent latitude (EqL) [*Butchart and Remsberg*, 1986], rather than geographic latitude. The data have been interpolated to the 585 K potential temperature (θ) surface, near the peak in the HNO_3 profile. The temperatures used for the interpolation to θ surfaces are taken from the U.K. Met Office analyses [*Swinbank and O'Neill*, 1994]; PV is also calculated from Met Office fields.

[9] For clarity of presentation, small data gaps of a few days or less have been filled by running the daily averages through a Kalman smoother. The Kalman smoother is an extension of the well-known Kalman filter that is particularly appropriate for postprocessing sequential data, when the best estimate of a quantity at a given time is obtained by considering measurements made both before and after that

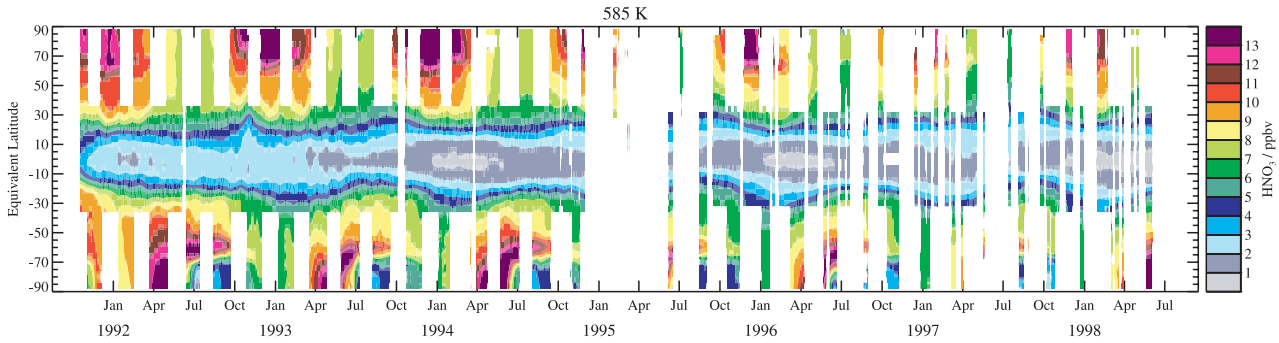

Figure 1. Time series over 7 years of MLS v6 HNO_3 at 585 K as a function of equivalent latitude (EqL). Small data gaps have been filled by running the daily vortex averages through a Kalman smoother (see text).

time [e.g., *Rodgers*, 2000]. The filter is run both forward and backward in time over the entire set of measurements, and the estimates from the two passes are then combined with appropriate weights to provide an overall estimate based on all of the data. A tunable parameter, often called the drift rate, describes our confidence in the use of the data from one day as an estimator of the data on another day. Smaller values of this parameter widen the "window of influence" that an individual point has on the filtered data, leading to results that represent broader averages and are thus smoother. That is, if the value of the drift rate is set too small, then the Kalman smoother produces output that is too smooth and, in the extreme case, tends toward an estimate of the mean over the entire input data set rather than following the point-to-point variations in the measurements. Conversely, if the value of the drift rate is set too large, then the Kalman smoother produces results similar to those obtained from a simple linear interpolation between adjacent measurements. For the results shown in Figure 1, the drift rate is set to 0.1 ppbv/d; this value enhances the readability of the contour plot in regions where measurements are not available on successive days while providing fields with minimal smoothing that resemble those plotted from the raw data extremely closely. In addition, blank spaces appear in the figure where the uncertainty in the Kalman-smoothed values exceeds a certain threshold (in this case, 0.9 ppbv), indicating that the interval is too far from actual measurements. Figure 1 clearly illustrates the interruption in MLS high-latitude data coverage arising from the regular UARS yaw maneuvers, the long data gap stretching from October 1994 through July 1995 caused by problems with the MLS scan system and the UARS batteries and solar array, and the generally decreasing MLS measurement frequency as the mission progressed.

[10] Many aspects of the stratospheric distribution of HNO_3 are evident in Figure 1. For example, HNO_3 abundances increase from low to high equivalent latitudes in both hemispheres and in all seasons, with the exception of the regions of strong polar stratospheric cloud (PSC) formation and denitrification in the Southern Hemisphere winter polar vortex (discussed further below). In addition, a pronounced seasonal cycle is evident at higher EqLs in both hemispheres, with a winter maximum and a summer minimum, whereas the seasonal cycle at lower latitudes is weak or nonexistent. Both the latitudinal and the seasonal variations in HNO_3 have been noted in numerous previous studies [e.g., *Santee et al.*, 1999, and references therein].

[11] Figure 1 provides a qualitative sense of the repeatability of the seasonal changes from year to year and the interhemispheric differences in the magnitude of those changes. Wintertime HNO_3 mixing ratios are primarily controlled by meteorological conditions: the strength of the diabatic descent, the permeability of the vortex, and the spatial extent and duration of low temperatures (which govern PSC formation). The Northern and Southern Hemispheres are characterized by distinctly different seasonal temperature patterns and vortex behavior. In the Arctic, lower stratospheric winter temperatures are ~15–20 K higher, on average, and the vortex is smaller, weaker, more distorted, more variable, and shorter-lived than in the Antarctic [e.g., *Andrews*, 1989; *Waugh and Randel*, 1999; *Waugh et al.*, 1999]. Whereas in the south, temperatures in the lower stratospheric winter polar vortex tend to exhibit a more or less steady decline to below the thresholds for PSC formation, in the north, greater dynamical activity is accompanied by rapid temperature variations. In general, these conditions lead to fewer, less persistent PSC events in the Arctic [e.g., *Poole and Pitts*, 1994; *Fromm et al.*, 1999]. During the mid-1990s, when the bulk of the UARS MLS HNO_3 measurements were made, however, the Arctic lower stratospheric vortex was unusually strong and long-lived [*Waugh et al.*, 1999], less variable from year to year, and atypically cold, with prolonged periods of temperatures low enough for extensive PSC formation [e.g., *Zurek et al.*, 1996; *Pawson and Naujokat*, 1999]. Nevertheless, the episodes of PSC activity in the Arctic were sufficiently localized and transient at this level in all of these years that none are discernible in the daily EqL averages shown here (though they are clearly visible in daily HNO_3 maps [e.g., *Santee et al.*, 1996, 1997, 1999]). In contrast, widespread PSC formation and denitrification are observed in the Antarctic in every year. (Note that since MLS is sensitive only to gas-phase HNO_3, MLS measurements alone cannot be used to distinguish temporary HNO_3 sequestration in PSCs from permanent denitrification, the removal of reactive nitrogen from the stratosphere through the sedimentation of PSCs; however, the occurrence of denitrification can be inferred from the persistent depression in gas-phase HNO_3 concentrations in November, well after the strato-

sphere has warmed above PSC existence thresholds [*Santee et al.*, 1995, 1999].)

[12] As noted earlier, low latitudes exhibit negligible HNO_3 seasonal variation. Figure 1 does, however, suggest that HNO_3 abundances at low EqLs are slightly elevated for the first ~1.5 years of the mission. One caveat in interpreting this plot is the ~2–3 ppbv high bias present in individual MLS HNO_3 measurements in the equatorial regions for the first ~100 days (up to January 1992), an artifact induced by enhanced stratospheric SO_2 from the eruption of Mount Pinatubo (section 2; see also *Livesey et al.* [2003]). The residual SO_2 from Pinatubo was almost entirely confined to the latitude band between 30°S and 15°N at this time [*Read et al.*, 1993] and did not affect midlatitude MLS HNO_3 retrievals. We attribute the persistent enhancement in HNO_3 at midlatitudes, and at low latitudes after the first few months, to the heterogeneous hydrolysis of N_2O_5 on volcanic aerosol [e.g., *Hofmann and Solomon*, 1989; *Brasseur and Granier*, 1992; *Webster et al.*, 1994; *Rinsland et al.*, 1994, 2003], with the decline in HNO_3 values after mid-1993 resulting from the decay of this aerosol [e.g., *Thomason et al.*, 1997; *Bauman et al.*, 2003]. Gradual recovery from Pinatubo-induced HNO_3 enhancement has also been seen in ground-based column amounts [e.g., *Koike et al.*, 1994; *David et al.*, 1994; *Slusser et al.*, 1998; *Rinsland et al.*, 2003] and UARS CLAES HNO_3 measurements [*Kumer et al.*, 1996], and trends in MLS HNO_3 data have also been discussed by *Randel et al.* [1999].

[13] The enhancement in HNO_3 in the early part of the mission is washed out when 7 years of data are averaged together to produce composite fields, as shown in Figure 2. Time series are shown for eight θ surfaces close to the standard UARS pressure levels used for the MLS v5 retrievals; it should be noted, however, that because of the vertical resolution of the data the HNO_3 values obtained at these levels are not completely independent. Because a given UARS yaw period starts ~5 days earlier in each succeeding year, the data gaps visible in Figure 1 are shortened when several years of measurements are averaged together. Averaging does not remove the gaps entirely, however, so to eliminate breaks in the composite fields, Kalman smoothing has been applied to the averaged HNO_3 values at each level. In order to ensure that one anomalous day/year does not dominate the climatological fields, a greater degree of smoothing (using a drift rate of 0.05 ppbv/d) has been applied to these averages than was used in Figure 1.

[14] We explored the validity of the Kalman smoothing approach in constructing these composite fields by comparing the results in Figure 2 to those obtained using a simple boxcar average. That is, we divided the annual cycle into a series of 5-day bins, populated these bins with data from all the years (an individual year thus contributed data from between 0 and 5 days to each bin), and then averaged together the data from all years in each bin. The morphologies of the fields constructed in this manner (not shown) are extremely similar to the ones in Figure 2. Because the Kalman smoother is mathematically superior in its handling of missing data, we have chosen to present the filtered data for these composite fields rather than the results from boxcar averages, but we stress that the smoothing has in no way distorted the inherent patterns in the data. Unlike in Figure 1, where intervals far from actual measurements have been blanked out, in the composite fields shown in Figure 2, the regions in which the estimated precision of the interpolated values is poor (i.e., greater than 0.5 ppbv) are denoted by paler colors. In addition, overlaid on these panels are contours (black lines) indicating where fewer than three distinct years contributed data to the 5-day boxcar averages. In most cases the regions of large uncertainty in the Kalman-smoothed values are not exactly coincident with those in which the 5-day boxcar window encompassed data from fewer than 3 years; although the black contours frequently enclose a greater area, under circumstances when the available MLS data on these days are limited or are of lesser quality, the pale regions can be larger. Outside of the regions characterized by either large uncertainties in the Kalman-filtered data or fewer than 3 years of available MLS data (i.e., throughout the tropics and at middle and high latitudes alternating with the UARS yaw cycle), the composite fields in Figure 2 can be considered climatologies.

[15] Figure 2 shows that weak seasonal patterns are present in HNO_3 at middle and high latitudes up to at least 960 K (~34 km). Microphysical model calculations [e.g., *Mills et al.*, 1999; *de Zafra and Smyshlyaev*, 2001] have indicated that the formation of small sulfate particles can lead to enhanced aerosol surface area in the winter polar regions up to or even slightly above 35 km. Conversion of NO_2 into N_2O_5 followed by heterogeneous hydrolysis of N_2O_5 to HNO_3 on sulfate aerosols [e.g., *Austin et al.*, 1986], coupled with the cessation during polar night of HNO_3 loss through photolysis and reaction with OH, leads to wintertime increases in HNO_3 throughout the lower and middle stratospheric vortex (see, e.g., *McDonald et al.* [2000] for a more detailed discussion).

[16] A broad peak in the high-latitude HNO_3 profile is centered around 585 K, where mixing ratios in the two hemispheres are comparable. Maximum abundances at higher levels (655–960 K) are larger in the Antarctic than in the Arctic. This may reflect the fact that NO_2 abundances at these levels are frequently higher in the south than in the north [*Siskind et al.*, 1997; *Randall et al.*, 1998; *Rinsland et al.*, 1999] and/or that descent rates in the north are typically faster than those in the south throughout the winter [e.g., *Manney et al.*, 1994], bringing down more air with lower HNO_3 abundances to these levels. In contrast, below the profile peak (420–520 K), maximum mixing ratios are larger in the north than in the south. This may again be a consequence of more vigorous descent in the north. In addition, extensive and persistent PSC activity acts to reduce HNO_3 abundances throughout the Antarctic vortex core, where the signature of HNO_3 depletion is seen over the range from 420 to 840 K. In the north, maximum abundances are reached at all levels in midwinter (December or early January), whereas in the south, PSC formation and denitrification start to reverse the seasonal increase in HNO_3 in early winter (May). Minimum temperatures are lower in the Antarctic vortex core than they are near the edge, leaving a band of higher HNO_3 along the vortex rim (the so-called "collar" region [*Toon et al.*, 1989]). Nevertheless, temperatures low enough to trigger significant growth of large PSC particles do extend into the vortex edge region, and it is likely that some degree of local denitrification takes place

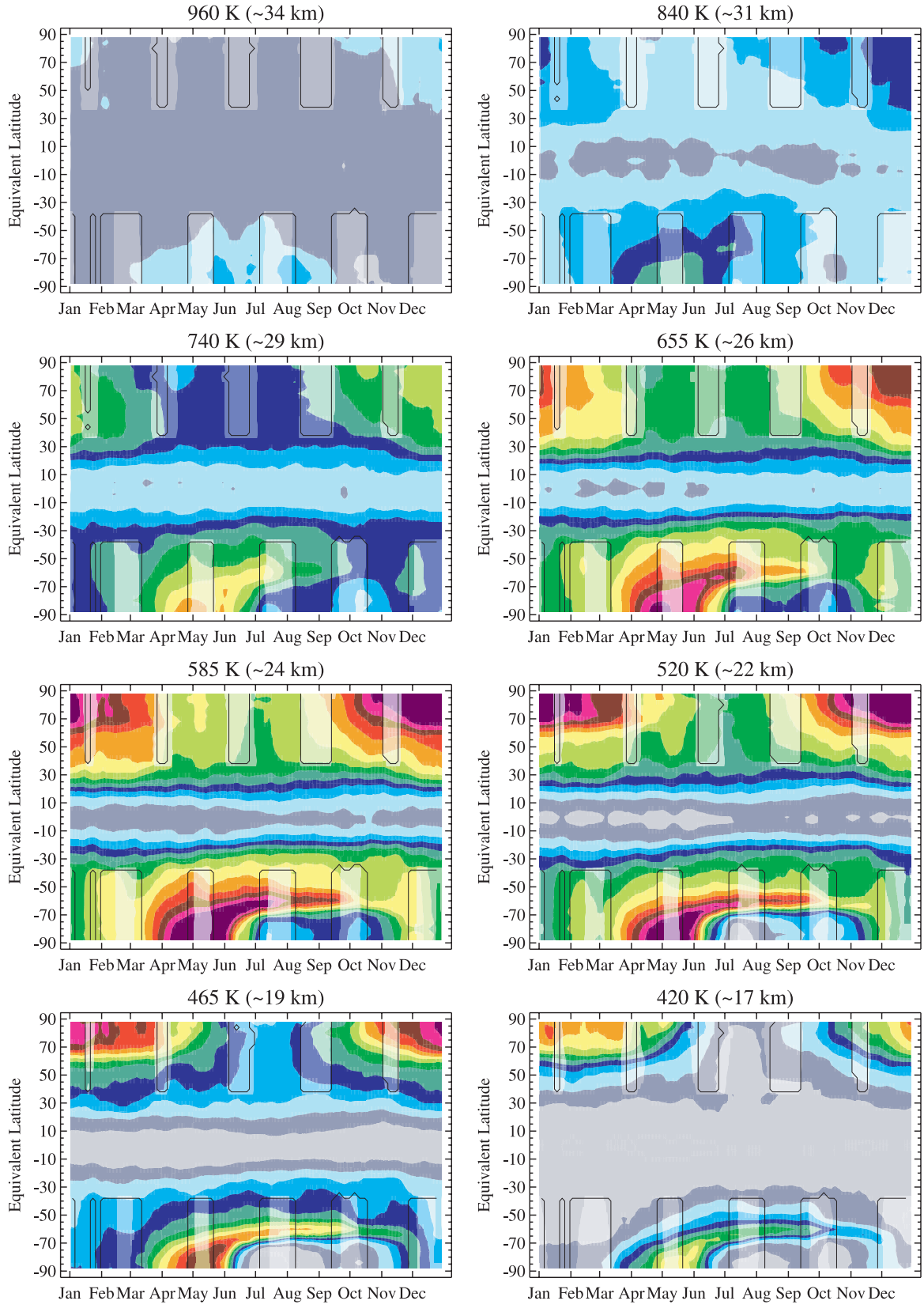
960 K (~34 km)
840 K (~31 km)
740 K (~29 km)
655 K (~26 km)
585 K (~24 km)
520 K (~22 km)
465 K (~19 km)
420 K (~17 km)
Equivalent Latitude
90 70 50 30 10 -10 -30 -50 -70 -90
Jan Feb Mar Apr May Jun Jul Aug Sep Oct Nov Dec
1 2 3 4 5 6 7 8 9 10 11 12 13
HNO3 / ppbv

Figure 2

there. Alternatively, although large-scale mixing between the vortex core and edge regions is limited in the Antarctic until late winter/spring [e.g., *Schoeberl et al.*, 1992; *Bowman*, 1993; *Lee et al.*, 2001], transport of severely denitrified air from the vortex interior may lead to some dilution of HNO_3 values in the collar region. All of these factors may play a role in the observed interhemispheric difference in the maximum abundances at the lowest levels.

[17] Figure 3 also shows time series of MLS HNO_3 both for individual years and averaged together to produce composite fields, but in this case, the data have been averaged over the area encompassed by a certain EqL contour and displayed as a function of θ. In other words, the values in Figure 3 are akin to vortex averages, except that they have been calculated over a fixed areal extent, rather than within a fixed PV contour, and are thus more relevant during the late spring and summer seasons when the area within a given PV contour may shrink substantially or even disappear. Unlike zonal means calculated over geographic latitude, however, they do not merge HNO_3 abundances measured inside and outside the winter vortex. To more closely approximate a vortex average when HNO_3 is enhanced in winter, different EqL contours have been used to define the averages in the two hemispheres; in the north the 65° EqL contour is situated in the region of strong PV gradients defining the winter vortex edge throughout the vertical domain considered here, whereas in the south the 60° EqL contour provides a similar relationship to the vortex edge.

[18] The influence of diabatic descent is clearly seen in the downward tilt of the HNO_3 contours in Figure 3, especially at higher altitudes. Although the Antarctic polar vortex starts to develop in the midstratosphere in March/April [e.g., *Manney and Zurek*, 1993; *Waugh and Randel*, 1999], the effects of confined descent are not immediately evident at these levels. Figure 3 shows that HNO_3 mixing ratios at the upper levels remain relatively constant or even increase slightly through middle to late June, with a steep downward trend in the HNO_3 contours appearing only in late June or July. Similar behavior has been observed around 30 km in GBMS HNO_3 measurements obtained from South Pole Station [*de Zafra et al.*, 1997; *McDonald et al.*, 2000]; *de Zafra et al.* [1997] attribute the delay in the downturn in the HNO_3 isopleths to the continuing conversion of NO_2 into HNO_3 as air descends from higher altitudes, with the direct effects of downward transport eventually becoming dominant. Dilution of the air brought down from above through mixing with air that has not experienced descent may also play a role in early fall, before the establishment of a strong transport barrier along the vortex edge. A corresponding evolution of the HNO_3 contours occurs in the Northern Hemisphere. In contrast to the Antarctic lower stratosphere, where it becomes obscured by the onset of denitrification, in the Arctic a clear signature of descent is apparent throughout the winter over the entire altitude range.

[19] A few other aspects of Figure 3 are worth noting. Although we have tried to minimize the influence of any particular year by applying slightly stronger smoothing in calculating the overall averages (as discussed in connection with Figure 2), it is clear that the anomalously high values of HNO_3 measured in late spring and summer 1991–1992 have skewed the Southern Hemisphere composite field. As will be discussed further below, the HNO_3 enhancement during the first months of MLS measurements most likely arises from heterogeneous processing on volcanic aerosols in the wake of the Mount Pinatubo eruption the previous June. In addition, we note that in some years a sharp increase in HNO_3 abundances occurs at the highest levels (above 900 K) in midwinter (e.g., late December 1992 in the north and late June 1993 in the south). This feature, which shows up weakly in the composite fields, probably represents the lowermost portion of the significant midwinter HNO_3 enhancement that has been observed over the ~35–50-km altitude range in GBMS [*de Zafra et al.*, 1997, 2003; *McDonald et al.*, 2000; *de Zafra and Smyshlyaev*, 2001], UARS CLAES [*Kawa et al.*, 1995], and Limb Infrared Monitor of the Stratosphere (LIMS) [*Austin et al.*, 1986] data. This enhancement has been successfully modeled by *de Zafra and Smyshlyaev* [2001] using heterogeneous reactions on sulfate aerosols below ~37 km supplemented by ion cluster chemistry extending to ~45–50 km when a sufficiently large downward flux of NO_2 from the polar winter mesosphere (arising from geomagnetic activity) is included.

[20] To take a more quantitative look at interannual and interhemispheric differences in the HNO_3 seasonal cycle, the data from each day are binned into 5° EqL bands and averaged; results are shown in Figure 4 for 7 years at 585 K in 10 EqL bands in both hemispheres. A similar plot showing daily zonal mean values calculated over geographic latitude was presented for the 465-K level by *Santee et al.* [1999]. As discussed in that paper, only a faint seasonal cycle (~2 ppbv or less) is present at the lowest latitudes, where interannual variability and interhemispheric differences are also minimal. The magnitude of variability, both day-to-day and year-to-year, increases with increasing EqL and is quite considerable in the winter vortex core in both hemispheres.

[21] The large disparity in the seasonal progression of vortex HNO_3 in the two hemispheres is readily seen in Figure 4. In the fall, Antarctic HNO_3 abundances at the highest EqLs exceed those in the Arctic by as much as 2 ppbv, as the developing vortex deepens more rapidly in the south [*Manney and Zurek*, 1993; *Waugh and Randel*, 1999] and provides a stronger barrier to mixing, allowing the effects of confined descent to raise HNO_3 concentrations at this level. By early June, however, a steep decreasing trend becomes apparent in the south in every year, and the

Figure 2. Composite MLS v6 HNO_3 fields as a function of EqL and time at eight potential temperature levels between 960 and 420 K, derived by averaging together the results for seven individual years at each level. To fill in breaks arising from data gaps, Kalman smoothing has been applied to the averaged HNO_3 values at each level; paler colors denote the regions in which the estimated precision of the interpolated values is poor (i.e., no MLS data are available). Overlaid in black are contours delimiting the regions in which data from fewer than three distinct years contributed to the averaged values (see text).

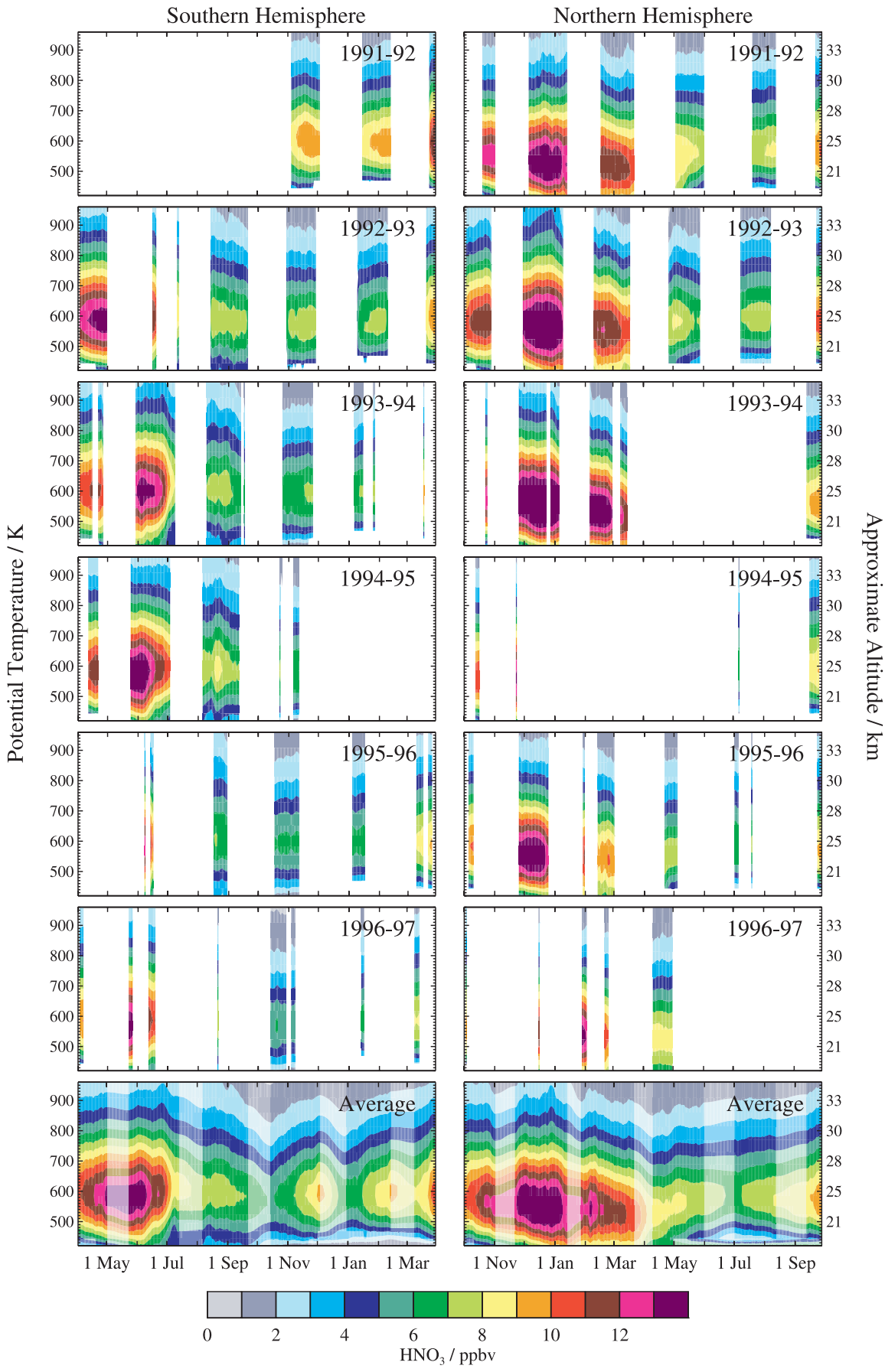
Southern Hemisphere
Northern Hemisphere
1991-92
1992-93
1993-94
1994-95
1995-96
1996-97
Average
Potential Temperature / K
Approximate Altitude / km
900
800
700
600
500
33
30
28
25
21
1 May
1 Jul
1 Sep
1 Nov
1 Jan
1 Mar
0
2
4
6
8
10
12
HNO_3 / ppbv

Figure 3

HNO_3 abundances in the two hemispheres begin to depart substantially. Virtually complete removal of gas-phase HNO_3 occurs at the highest southern EqLs in July from 420 to 840 K (not shown). Note that the MLS retrieval algorithms occasionally produce negative mixing ratios, especially for noisy retrievals such as HNO_3 when values are very low; though unphysical, these have been retained in order to avoid introducing biases into the averages. Because of UARS yaw maneuvers and other data gaps, the maximum HNO_3 mixing ratios attained in May were never captured in the MLS data set, but PSC formation and denitrification are estimated to decrease the daily average HNO_3 values by at least 16 ppbv at 585 and 520 K in some years (where the depletion in a given year is defined as the difference between the maximum and minimum observed values in that year) and as much as 6 ppbv at 840 K. Because of the progressively worse vertical resolution of the MLS HNO_3 data with altitude, however, values at the topmost levels may be significantly influenced by those at lower levels. In contrast, even in the coldest Arctic winters (e.g., 1995–1996 and 1996–1997), HNO_3 depletion of at most 8–10 ppbv is seen in the daily averages in February from 420 K (not shown) to 585 K (the highest level at which a PSC-related decline in HNO_3 values can be discerned in the north). In keeping with the smaller size of the Arctic vortex [*Waugh and Randel*, 1999], HNO_3 depletion is also more limited geographically in the north, extending no farther than 70°–75° EqL even at 465 K, whereas in the south it occurs into the 65°–70° EqL band, albeit less dramatically than at higher EqLs. Of course, it must be borne in mind that the inferences drawn from Figure 4 are based on averages taken over EqL bands and that HNO_3 removal processes may be operating on spatial scales not detectable in these averages (or indeed in the MLS data at all).

[22] In the Antarctic, HNO_3 concentrations at 585 K have begun to rebound by the beginning of the south-viewing observation period in early to mid-August, and they continue to increase through the November observation period. Evaporation of remaining PSCs when temperatures rise above PSC existence thresholds may play a role in the springtime HNO_3 increase. In addition, HNO_3 is so severely depleted inside the Antarctic vortex at this level that mixing with lower latitude air as the vortex erodes in late spring causes the mixing ratios to rise at the highest EqLs. In contrast, Arctic HNO_3 decreases fairly steadily from March to May, through a combination of the effects of mixing after vortex breakdown and, after sunrise, photolysis. Note that averaging over EqL may obscure to some extent the effects of photolysis in the spring, especially in the Northern Hemisphere where the EqL contours are often not well aligned with geographic latitude. Mixing ratios in both hemispheres level off at comparable summertime values in January/July. On the basis of the result that zonal-mean HNO_3 values at 465 K for the two hemispheres are virtually indistinguishable at latitudes equatorward of ~65°, even during winter, and that high-latitude HNO_3 recovers to similar values at the end of every winter in both hemispheres, *Santee et al.* [1999] concluded that the effects of severe denitrification are confined in both space and time to the regions poleward of 65°S during austral winter and early spring. The EqL averages shown in Figure 4 and those at other θ levels support this conclusion.

[23] The Antarctic daily averages for 1991–1992 and much of 1992–1993 particularly stand out in many EqL bins in Figure 4. For the first few months after the eruption of Mount Pinatubo in June 1991, the strong Antarctic vortex effectively blocked dispersal of volcanic aerosol into the southern polar regions, but aerosol loading at southern midlatitudes (<60°S) was significantly enhanced up to 30 km by September 1991 [*Trepte et al.*, 1993; *Thomason et al.*, 1997; *Bauman et al.*, 2003]. The MLS data obtained at southern midlatitudes at the beginning of November 1991 indicate HNO_3 abundances that are well outside the envelope of typical values. At the highest EqLs, however, HNO_3 mixing ratios are not anomalous until mid-November, when they suddenly increase substantially. The timing of this abrupt increase coincides with the breakdown of the polar vortex in the lower stratosphere this year [*Waugh and Randel*, 1999; *Waugh et al.*, 1999], allowing a dramatic increase in the aerosol loading at high southern latitudes [e.g., *Thomason et al.*, 1997; *Bauman et al.*, 2003]. The atypically high HNO_3 concentrations in the southern middle and high latitudes are most likely a consequence of perturbations in reactive nitrogen chemistry induced by the injection of volcanic aerosol [e.g., *Hofmann and Solomon*, 1989; *Brasseur and Granier*, 1992; *Webster et al.*, 1994; *Rinsland et al.*, 1994]. The aerosol enhancement at the highest southern latitudes was relatively short-lived, however, and had dissipated to a large extent by the beginning of June 1992 [*Thomason et al.*, 1997; *Bauman et al.*, 2003], when MLS HNO_3 values at the highest EqLs return to more normal values. Mixing ratios in some midlatitude EqL bins remain elevated for several months longer, consistent with residual volcanic aerosol at lower latitudes [e.g., *Bauman et al.*, 2003].

[24] A fairly similar pattern of Southern Hemisphere Pinatubo-related HNO_3 enhancement and recovery to that at 585 K shown in Figure 4 is observed up to 840 K (not shown), but not at 420 or 465 K, where the intact vortex was still inhibiting massive intrusion of volcanic aerosol in November 1991, resulting in only moderate enhancement in high-EqL HNO_3 at these levels (not shown). Unlike at

Figure 3. Averages of MLS v6 HNO_3 calculated within the (left) 60° EqL contour for the Southern Hemisphere and (right) 65° EqL contour for the Northern Hemisphere as a function of potential temperature from 420 to 960 K. The top six rows show data from individual years; because of decreasing measurement frequency the data from 1997–1998 have been omitted. Small data gaps in these panels have been filled by running the daily vortex averages through a Kalman smoother. The bottom row shows composite fields derived by averaging together the results for the individual years. As in Figure 2, breaks in the composite fields have been eliminated by applying a greater degree of Kalman smoothing than was used for the individual years in the panels above; paler colors denote the regions in which the estimated precision of the interpolated values is poor (i.e., no MLS data are available). The approximate altitude scale is calculated using the nonlinear formula of *Knox* [1998].

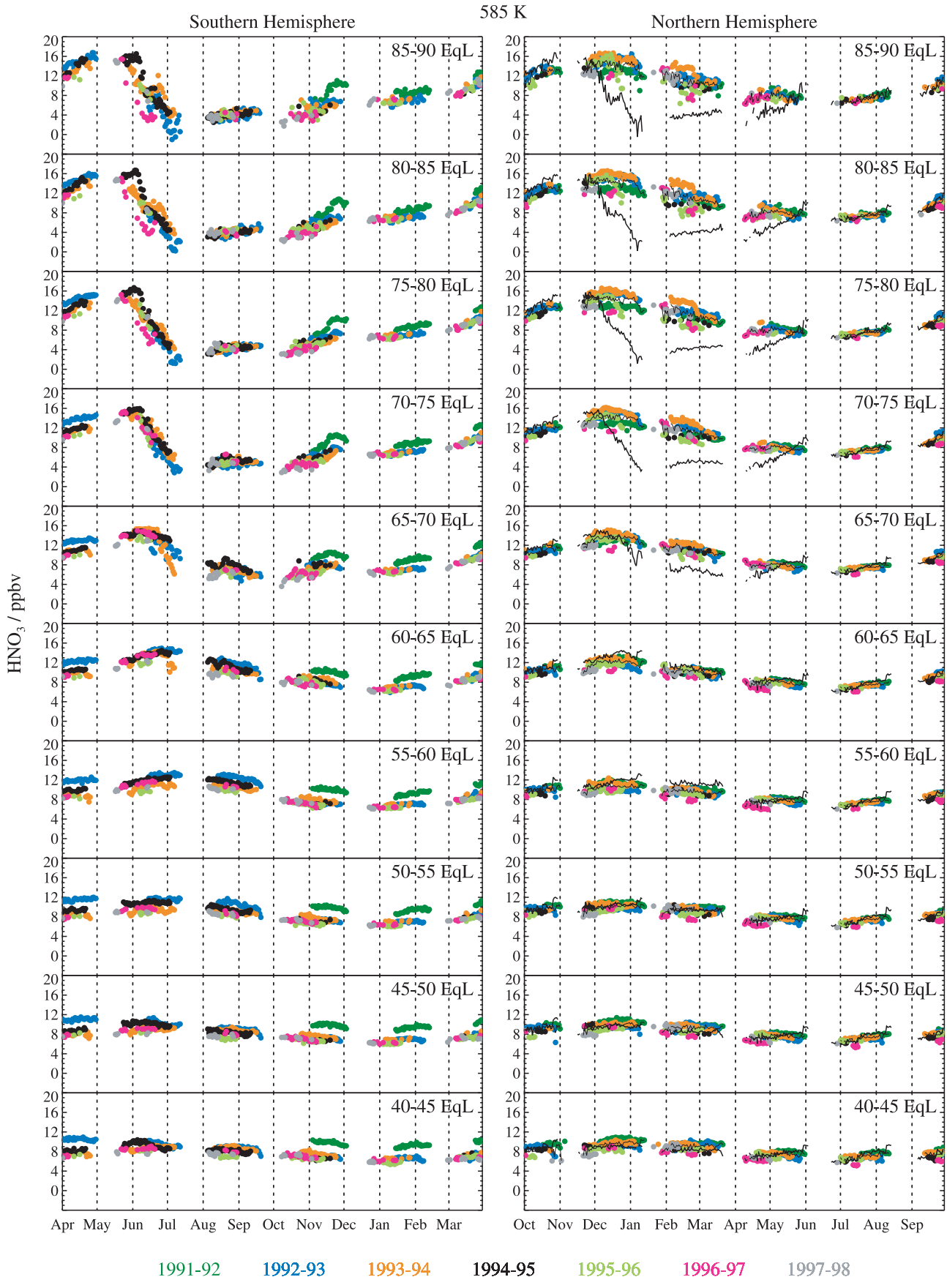
585 K
Southern Hemisphere
Northern Hemisphere
85-90 EqL
80-85 EqL
75-80 EqL
70-75 EqL
65-70 EqL
60-65 EqL
55-60 EqL
50-55 EqL
45-50 EqL
40-45 EqL
HNO3 / ppbv
0 4 8 12 16 20
Apr May Jun Jul Aug Sep Oct Nov Dec Jan Feb Mar
Oct Nov Dec Jan Feb Mar Apr May Jun Jul Aug Sep
1991-92
1992-93
1993-94
1994-95
1995-96
1996-97
1997-98

Figure 4

Table 2. Representative Days for Each Season

Hemisphere	Fall	Early Winter	Late Winter	Spring
North	1 October	20 December	25 February	30 April
South	1 April	15 June	25 August	4 November

585 K, at these levels lingering aerosol enhancement [e.g., *Bauman et al.*, 2003] continued to affect HNO_3 abundances slightly at lower EqLs through the beginning of 1993. Interestingly, however, at no time was the influence of the Pinatubo aerosol on MLS HNO_3 concentrations at 420 and 465 K as substantial as it was at higher altitudes. This may be a result of the fact that at midlatitudes the conversion of NO_2 to HNO_3 saturates at relatively low aerosol loadings at lower altitudes, whereas at higher altitudes much larger aerosol surface areas are required for saturation in the partitioning between NO_2 and HNO_3 to occur [e.g., *Mills et al.*, 1993]. Alternatively, it may be linked to differences in the availability of NO_2. Stratospheric NO_2 enhancements (abundances over those expected from N_2O oxidation) arising from the production of NO_x in the mesosphere through geomagnetic activity followed by descent are fairly regular occurrences [*Siskind et al.*, 1997, 2000; *Randall et al.*, 1998, 2001; *Rinsland et al.*, 1999]. In particular, a layer of enhanced NO_2 in the Southern Hemisphere midstratosphere was seen in UARS Halogen Occultation Experiment (HALOE) data in November 1991 [*Siskind et al.*, 2000]. Because of their timing, however, such NO_2 enhancements typically have little effect on the lower stratosphere as the vortex dissipates before descent can bring air with elevated NO_2 down to the lowest levels [e.g., *Randall et al.*, 1998].

[25] In contrast to the Southern Hemisphere, HNO_3 mixing ratios at 585 K at northern middle and high latitudes were not substantially affected by Pinatubo. Although significant amounts of volcanic aerosol were dispersed poleward during the 1991 boreal autumn at lower altitudes, above ~24–25 km the aerosol enhancement north of 45°–50°N was relatively moderate and brief [e.g., *Thomason et al.*, 1997; *Bauman et al.*, 2003]. In addition, although the transport of enhanced NO_2 from the mesosphere is well documented in the Antarctic vortex, there is little or no evidence of anomalously high NO_2 in the Arctic stratosphere [*Siskind et al.*, 1997; *Randall et al.*, 1998; *Rinsland et al.*, 1999], so there may simply have been less NO_2 to be converted to HNO_3 in the north. *Kumer et al.* [1996] also report a distinct decreasing trend in calculated UARS CLAES HNO_3 column amounts in the Southern Hemisphere over the period from February 1992 to February 1993, which they attribute to recovery from Pinatubo-related enhancement, but a much weaker decreasing trend in the northern tropics and actually a slight increase in HNO_3 column amounts over this period at northern middle and high latitudes. *Kumer et al.* [1996] suggest the quasi-biennial oscillation (QBO) as a plausible mechanism for inducing the apparent hemispheric asymmetry in the CLAES HNO_3 trends during this period.

3.2. Seasonal Snapshots

[26] We focus in this section on defining the typical behavior of HNO_3 during several intervals of particular interest in the annual cycle. As shown by *Santee et al.* [1999] and seen also in the previous figures, HNO_3 mixing ratios are uniformly low throughout the summer hemisphere and exhibit little day-to-day, interannual, or interhemispheric variability; therefore the summertime HNO_3 distribution is not considered further here. Climatological HNO_3 fields representative of four "seasons" (fall, early winter, late winter, and spring) in each hemisphere are produced by averaging together all the data obtained within a 5-day interval on either side of the dates given in Table 2 over a period of 7 years. The central dates for these intervals are chosen to maximize data coverage, taking into account missing data and the UARS yaw state, while still allowing comparison of equivalent seasons in the two hemispheres. For any individual year the minimum number of days contributing to the seasonal averages is 2, and the maximum is 11; data from 5–7 individual years, for a total of 34–51 days, are combined for each of the overall seasonal averages. The length of the intervals is limited to 11 days because meteorological conditions, and hence the HNO_3 distribution, can change rapidly, especially during spring and fall. Similarly, significant changes in high-latitude HNO_3 abundances over the course of the winter dictate the division of this season into two separate periods. In addition to averaging together the MLS HNO_3 data for these days, we also average the PV fields from the Met Office analyses. Two contours of PV are overlaid in Figures 5–7 (black lines in Figures 5 and 6 and white lines in Figure 7) to illustrate the typical size, shape, and strength of the polar vortex at each level and in each season.

[27] The vertical distribution of HNO_3 during these four seasons is illustrated in the equivalent latitude/potential temperature (EqL/θ) representations of Figures 5 and 6. HNO_3 exhibits little vertical, seasonal, or interannual variability in the tropics. The peak in the vertical profile occurs around 700–750 K near the equator and moves steadily down in altitude to ~550 K in the vortex core in midwinter, as first noted in LIMS data [*Gille and Russell*, 1984; *Gille et al.*, 1984]. Just inside the vortex edge, the latitudinal gradients are very strong, especially near the profile peak at ~600 K; the vertical gradients in this region are also very strong. The pronounced dip in the HNO_3 contours along the vortex edge is a signature of strong descent. A similar pattern of HNO_3 isopleths that slope downward and poleward in the lower stratosphere but that are relatively flat in the middle stratosphere was also reported in LIMS [*Austin et al.*, 1986] and ATMOS [*Manney et al.*, 1999] measurements. That the peak in the HNO_3 profile typically occurs at slightly lower

Figure 4. Time series of MLS v6 HNO_3 at 585 K for both the (left) Southern and (right) Northern Hemispheres. Daily means were calculated by binning the measurements into 5° EqL bands and averaging; different years are represented by different colors as indicated in the legend. Dashed vertical lines demark calendar months. Overall daily averages calculated from the Southern Hemisphere data points in every year are overlaid on the Northern Hemisphere plot as a thick black line (shifted by six months so that comparable seasons are aligned). To facilitate comparison, the overall daily averages calculated from the Northern Hemisphere data points are also overlaid on the Northern Hemisphere plot as a thin black line.

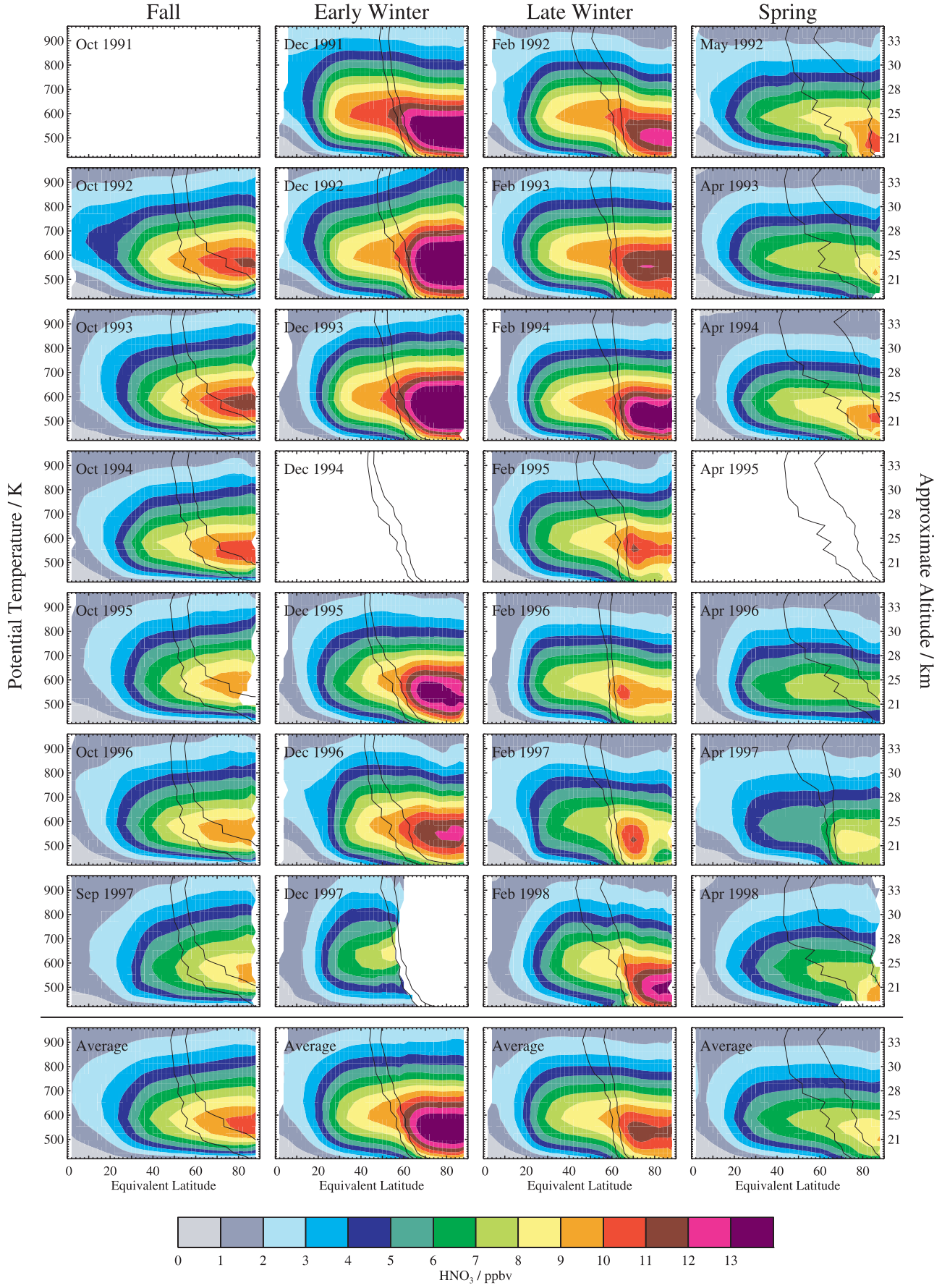
Fall
Early Winter
Late Winter
Spring
Oct 1991
Dec 1991
Feb 1992
May 1992
Oct 1992
Dec 1992
Feb 1993
Apr 1993
Oct 1993
Dec 1993
Feb 1994
Apr 1994
Oct 1994
Dec 1994
Feb 1995
Apr 1995
Oct 1995
Dec 1995
Feb 1996
Apr 1996
Oct 1996
Dec 1996
Feb 1997
Apr 1997
Sep 1997
Dec 1997
Feb 1998
Apr 1998
Average
Potential Temperature / K
Approximate Altitude / km
Equivalent Latitude
HNO_3 / ppbv

Figure 5

altitudes in the Northern Hemisphere is most likely a consequence of stronger descent there than in the Southern Hemisphere [e.g., *Manney et al.*, 1994].

[28] A striking degree of interannual variability in the seasonal buildup and depletion of HNO_3 occurs in both hemispheres. One caveat in interpreting these plots is that the gridding and averaging procedures smear out highly localized and transient phenomena such as PSC events; this problem is particularly acute in the Arctic, where PSCs are typically much less extensive and shorter-lived. The late February intervals in 1996 and 1997, however, were periods of extreme cold with fairly large pockets of substantially depleted HNO_3 [*Santee et al.*, 1996, 1997]. In fact, 20 February 1996 proved to be the coldest Arctic winter day in the entire UARS MLS data record, with the most Antarctic-like HNO_3 distribution. The 1996 low-HNO_3 region is not as apparent in these plots because the PSC episode was relatively transitory and about twice as many days as in 1997 contributed to the average in 1996. Compared with the Northern Hemisphere, the Southern Hemisphere displays as much (and perhaps even more) interannual variation in the maximum mixing ratios attained in fall and early winter and the spatial extent over which the largest abundances are found. Similarly, although severe HNO_3 loss is observed at high EqLs throughout much of the vertical range every year, the horizontal and vertical extent and the degree of depletion are also highly variable from year to year in the south.

[29] Finally, we present in Figure 7 a set of maps showing climatological HNO_3 fields for the four seasons in each hemisphere at three potential temperatures. Only the overall averages taken over the 7 years of data are shown. Looking first at the fall maps, although in some years HNO_3 mixing ratios are roughly equal in the two hemispheres (not shown), in the overall climatologies they are slightly larger in the south than in the north at all three levels. As indicated in the time series plots in section 3.1, substantial enhancement of HNO_3 is just starting at this time, as the conversion of N_2O_5 proceeds in darkness. The vortex has not yet developed at 465 K in the Northern Hemisphere, so that any air with higher HNO_3 brought down from above is probably diluted through mixing with lower latitude air. At 585 K the spacing of the PV contours implies a much stronger barrier to mixing in the Southern Hemisphere, with the effects of confined descent leading to correspondingly larger HNO_3 values there than in the north. In the midstratosphere the Arctic vortex on 1 October is approximately the same size and shape as the Antarctic vortex on 1 April [*Manney and Zurek*, 1993]. Nevertheless, HNO_3 mixing ratios that are, on average, larger suggest the occurrence of less mixing with extravortex air in the south even at this level, despite the fact that the climatological PV contours do not appear significantly different in the two hemispheres. Alternatively, more NO_2 may have been available for conversion in the south, as suggested earlier. On the other hand, there is a much greater degree of variability, both interannual and day-to-day, in the shape and position of the vortex in the north, particularly in early winter [*O'Neill and Pope*, 1990; *Waugh and Randel*, 1999]. Unlike the values shown in all previous plots, which were calculated over EqL and thus accounted for differences in vortex shape and position on the days being averaged, the averages of gridded fields displayed in these maps may reflect merged contributions from both vortex and extravortex air, even in regions situated within the climatological PV contours designating the vortex edge.

[30] Climatological HNO_3 values increase between fall and early winter at all levels in both hemispheres. Examination of maps for individual years (not shown), however, reveals that, while a substantial increase occurs in the Arctic in some years (e.g., 1992), little or no increase occurs in others (e.g., 1995 and 1996); a similar degree of interannual variability in the seasonal buildup of HNO_3 is seen in the Antarctic. These results underscore the extent to which a single year can influence climatological fields. Stronger descent in the Arctic leads to mixing ratios that are smaller at 740 K (above the profile peak) but larger at 465 K (below the peak) than in the Antarctic. In addition, the effects of HNO_3 sequestration in PSCs are already apparent in the Antarctic early winter maps at all three levels, particularly in the area between the Palmer Peninsula and the Greenwich Meridian, a region in which PSCs have been shown to form preferentially [*Watterson and Tuck*, 1989; *Poole and Pitts*, 1994; *Fromm et al.*, 1997].

[31] By late winter the signature of severe denitrification is apparent over much of the Antarctic vortex up to (and even above, not shown) 740 K. As discussed previously in section 3.1, extensive and persistent PSC formation reduces HNO_3 throughout the Antarctic lower stratospheric vortex, including (to a lesser extent than in the vortex core) the collar region. In contrast, the late winter HNO_3 distribution in the Arctic shows no suggestion of substantial denitrification at any level, although the climatology at 465 K does exhibit slightly depressed HNO_3 concentrations in the preferred PSC formation region between Greenland and Scandinavia. It should be noted, however, that even though this area is inside the climatological vortex, as mentioned earlier it is possible that in some years, low-latitude air poor in HNO_3 contributes to the averages there. Unlike at 585 and 740 K, where descent acts to reduce HNO_3 mixing ratios from their early winter values throughout the vortex (compare the tilt in the contours in Figure 3), at 465 K, descent should continue to increase HNO_3 through the winter. That 465 K abundances have declined slightly in late winter implies that the effects of ongoing sequestration in PSCs and/or denitrification are substantial enough to counteract replenishment by descent even in the Northern Hemisphere. Indeed, maps for individual years (not shown) indicate no significant decrease between early and late winter in the Arctic in 1993–1994 and 1997–1998, fairly

Figure 5. Equivalent latitude/potential temperature (EqL/θ) cross sections of MLS v6 HNO_3 in the Northern Hemisphere averaged over 11-day intervals in four "seasons" in each of 7 years (top seven rows). The bottom row shows climatologies derived by averaging together the results for the individual years; they represent averages over a total of 34–51 days, depending on the season (see text). The black lines represent two contours of Met Office potential vorticity (PV), scaled to give similar values throughout the θ domain.

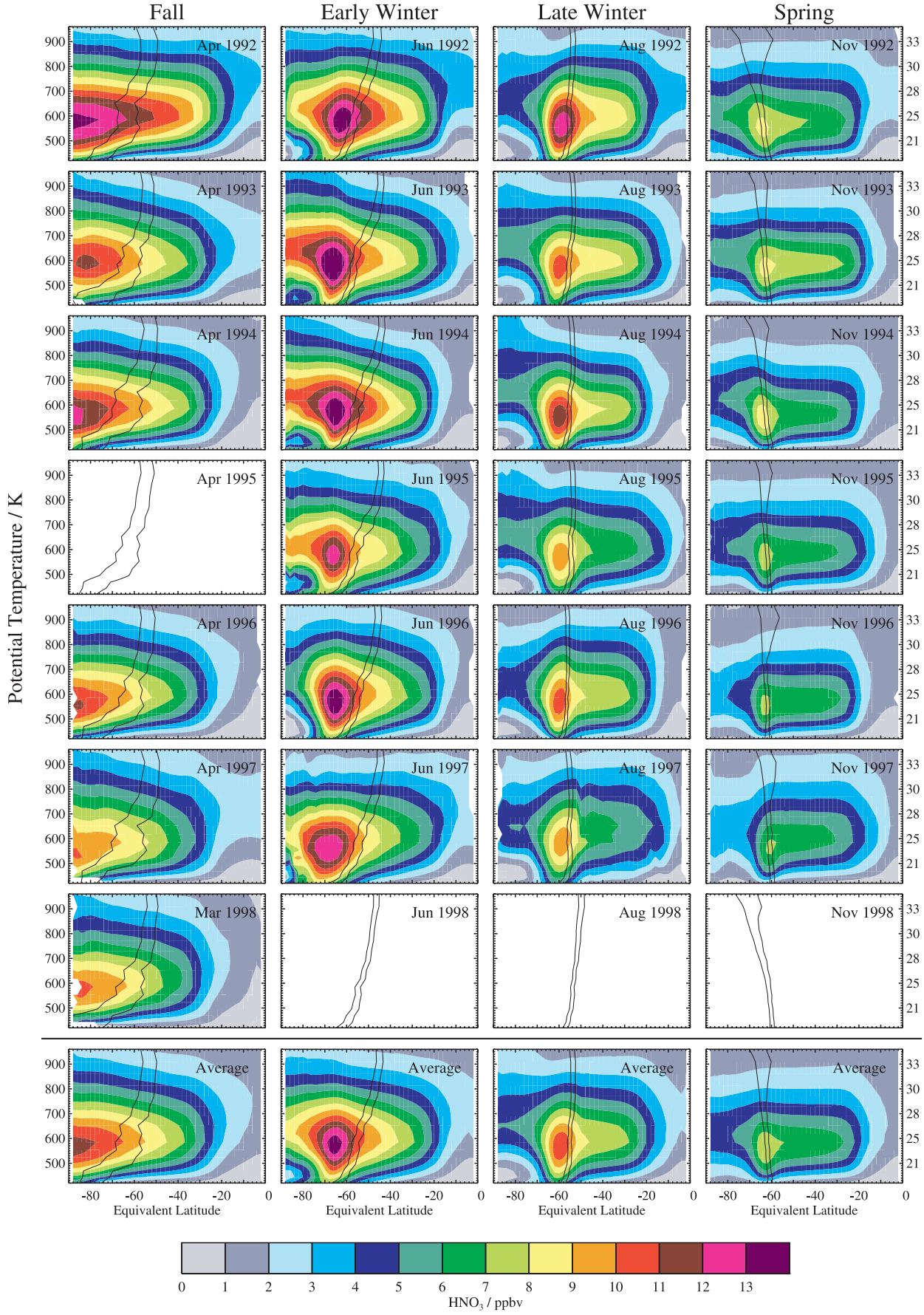

Figure 6. As in Figure 5, for the Southern Hemisphere.

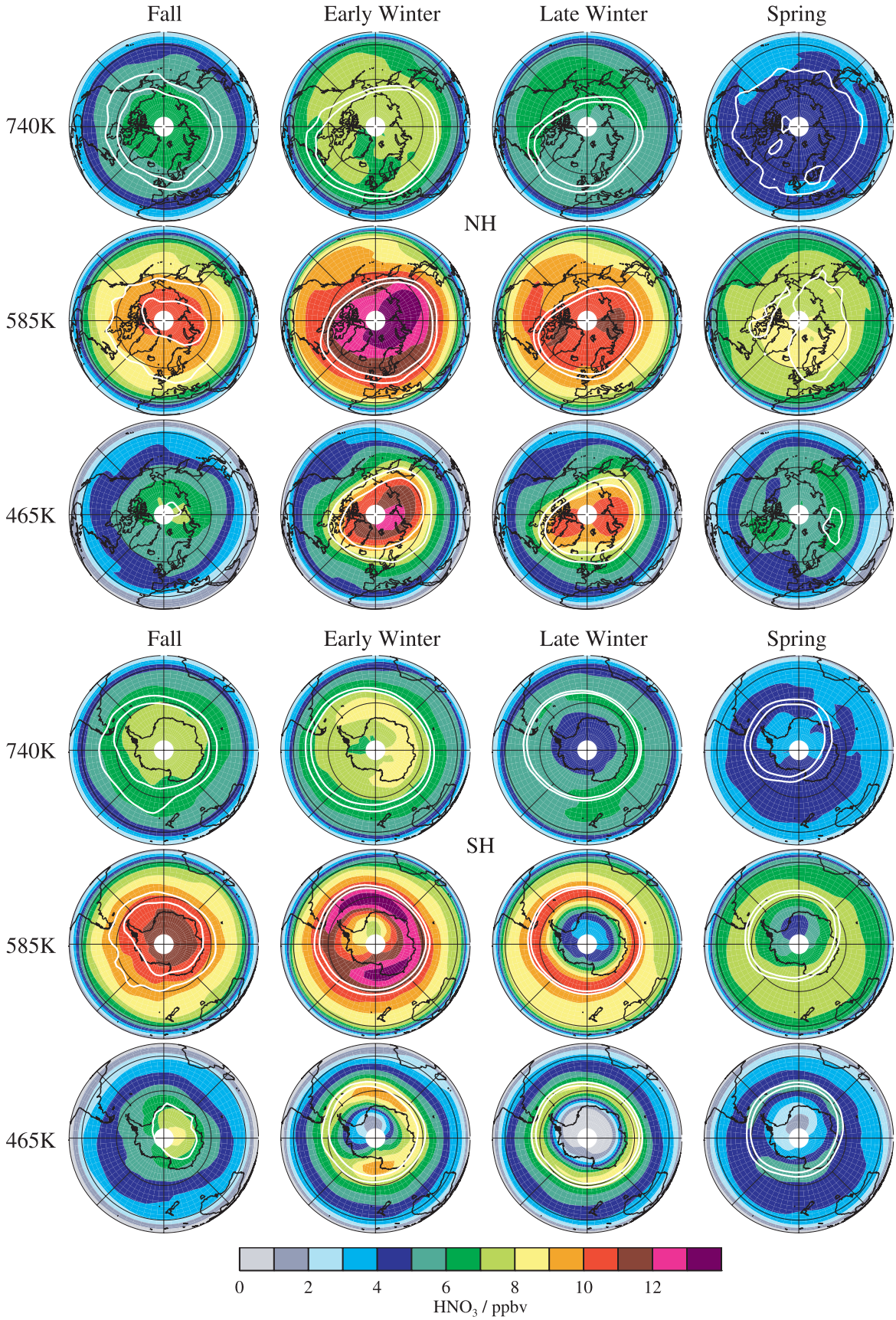
Fall
Early Winter
Late Winter
Spring
740K
585K
465K
NH
Fall
Early Winter
Late Winter
Spring
740K
585K
465K
SH
0
2
4
6
8
10
12
HNO3 / ppbv

Figure 7

warm years with little midwinter PSC activity, but considerable decreases in 1991–1992, 1992–1993, 1995–1996, and 1996–1997, years with very cold intervals between late December and late February. Significant variability in late winter vortex size, shape, and strength may also affect the climatological maps, as discussed above.

[32] In the spring the initiation of photolysis with returning sunlight reduces HNO_3 at all levels. The polar vortex erodes from the top down and typically dissipates in the lower stratosphere in late March or early April in the Arctic, whereas it typically remains robust in the lower stratosphere through early to middle December in the Antarctic [*Waugh and Randel*, 1999; *Waugh et al.*, 1999]. In the Northern Hemisphere the vortex stayed intact throughout the middle and lower stratosphere into early May in 1997 [*Coy et al.*, 1997]. In a few other years (e.g., 1992 and 1998), small vortex fragments maintained their identity in late April at least at 465 K, and HNO_3 enhancement persisted within these vortex remnants (not shown). In other years, however, the breakdown of the vortex led to rapid mixing with low-HNO_3 air by this time.

[33] The enduring depression in HNO_3 abundances in the Antarctic vortex in early November, after stratospheric temperatures have risen well above PSC existence thresholds in every year, confirms that the HNO_3 has been irreversibly removed from these levels through denitrification and is not simply still sequestered in extant PSCs. Indications of denitrification at 740 K show up more clearly in a few individual years (e.g., 1993, 1996, and 1997; not shown) but are weakly present in the climatological map. Although low, temperatures at these levels were not below the ice frost point in any of these years. Indeed, inspection of more than 10 years of analyses from the Met Office and more than 20 years of analyses from the National Centers for Environmental Prediction (NCEP) and the NCEP/National Center for Atmospheric Research Reanalysis reveals very little area with temperatures below the frost point at 15 hPa in most years and none at 10 hPa in any year (the 740-K θ surface corresponds to pressures of $\sim$10 hPa in the Southern Hemisphere early/late winter). Consistent with the meteorological conditions, satellite observations from MLS [*Stone et al.*, 2001], HALOE [*Rosenlof et al.*, 1997], and Polar Ozone and Aerosol Measurement (POAM) III [*Nedoluha et al.*, 2000, 2002] have shown that Antarctic dehydration is confined to levels below $\sim$23 km ($\sim$550 K). On the other hand, the area with temperatures persistently below the existence threshold for nitric acid trihydrate (NAT) PSCs for substantial periods is significant up to and even above 10 hPa in many years (depending on which meteorological analyses are used), and PSCs have occasionally been observed at altitudes as high as 28 km in early winter and midwinter (though not in late winter) [*Poole and Pitts*, 1994; *Fromm et al.*, 1997]. On the basis of UARS MLS and CLAES measurements, *Tabazadeh et al.* [2000] argued that extensive denitrification precedes significant dehydration by a few weeks at 450 K in the Antarctic. The MLS HNO_3 data shown here imply that denitrification is an independent process that occurs in the absence of dehydration in the upper portions of the Antarctic lower stratosphere as well. Because of the relatively poor vertical resolution of the MLS HNO_3 data at the highest levels, however, the values at 655 or even 585 K may have a nonnegligible influence on the 740 K distribution, so that caution must be exercised in interpreting these maps. Nevertheless, the MLS data shown here provide further evidence that the processes of denitrification and dehydration are not strongly coupled.

4. Summary and Conclusions

[34] UARS MLS version 6 HNO_3 measurements were presented to provide an overview of the seasonal, interhemispheric, and interannual variations in the distribution of HNO_3 over seven annual cycles in the 1990s in both hemispheres throughout the lower and middle stratosphere from 420 to 960 K. Time series of different slices through the data were used to develop a comprehensive picture of the mean evolution of stratospheric HNO_3 during the UARS MLS time frame. Maps and equivalent latitude/potential temperature cross sections were shown to illustrate the typical behavior of HNO_3 during intervals of interest in the annual cycle. Composite/climatological fields were derived by averaging together the results for individual years.

[35] HNO_3 exhibits little vertical, seasonal, or interannual variability in the tropics. For the first $\sim$1.5 years of the mission, however, a persistent enhancement is seen, especially at low and middle latitudes, which we attribute to the heterogeneous conversion of N_2O_5 under conditions of high aerosol loading from the eruption of Mount Pinatubo. In particular, in the middle stratosphere and the upper portions of the lower stratosphere the MLS data obtained at southern midlatitudes at the beginning of November 1991 indicate HNO_3 abundances that are well outside the envelope of typical values. HNO_3 mixing ratios are not anomalous at the highest EqLs until mid-November, when the breakdown of the Antarctic vortex at these levels allows volcanic aerosol to penetrate to high latitudes. At the highest southern latitudes, aerosol enhancement at these levels largely dissipates, and MLS HNO_3 values relax to unperturbed values by the beginning of June 1992, whereas at some midlatitude EqLs, residual volcanic aerosol keeps mixing ratios elevated for several months longer. At the lowest levels (420 and 465 K), lingering aerosol enhancement continues to affect HNO_3 abundances slightly at lower EqLs through the beginning of 1993. At no time, however, is the influence of the Pinatubo aerosol on MLS HNO_3 concentrations as dramatic at these levels as it is at higher altitudes. In contrast to the Southern Hemisphere, HNO_3 mixing ratios at northern middle and high latitudes are not substantially affected by Pinatubo.

[36] HNO_3 abundances increase from low to high EqLs in both hemispheres at all levels and in all seasons, with the exception of the severely denitrified region inside the

Figure 7. Climatological maps of MLS v6 HNO_3 in the Northern (top three rows) and Southern (bottom three rows) Hemispheres for four "seasons" (see Table 2) at 740, 585, and 465 K. The white lines on each map represent two contours of Met Office PV, shown to indicate the approximate size and strength of the polar vortex.

Antarctic vortex. A pronounced seasonal cycle is present at middle and high EqLs in both hemispheres up to at least 960 K (~34 km), with a winter maximum and a summer minimum. Large interannual variability in the timing, magnitude, and duration of enhanced wintertime HNO_3 abundances is seen in both hemispheres, and the variability increases with increasing EqL. The peak in the vertical profile occurs around 700–750 K near the equator and moves steadily down in altitude to ~550 K in the vortex core in midwinter. Vortex mixing ratios near the peak are comparable in the two hemispheres. Above the peak, maximum abundances are larger in the Antarctic than in the Arctic, whereas below the peak maximum abundances are larger in the north. Maximum abundances are reached at all levels in the north in midwinter (December or early January), whereas PSC formation and denitrification start to reverse the seasonal increase in HNO_3 abundances in the south in early winter (May). Virtually complete removal of gas-phase HNO_3 occurs at the highest southern EqLs by July in every year throughout the lower stratosphere. In contrast, even in the coldest Arctic winters, HNO_3 depletion is modest and is also more limited in both horizontal and vertical extent. The slight decline in climatological abundances at the lowest levels between early and late winter, however, implies that, at least in some winters, ongoing sequestration in PSCs and/or denitrification are substantial enough to counteract replenishment by descent even in the Northern Hemisphere.

[37] The enduring depression in HNO_3 abundances throughout the still-intact Antarctic lower stratospheric vortex in early November, after stratospheric temperatures have risen well above PSC existence thresholds in every year, confirms that HNO_3 has been irreversibly removed from these levels through denitrification and is not simply still sequestered in extant PSCs. The EqL averages throughout the lower stratosphere shown here support the conclusions of *Santee et al.* [1999] that the effects of severe denitrification are confined in both space and time to the regions poleward of 65°S during austral winter and early spring. Indications of denitrification are present up to at least 740 K, well above the highest altitude (~550 K) at which dehydration is observed. Because of the relatively poor vertical resolution of the MLS HNO_3 data at the highest levels, however, the values at 655 or even 585 K may have a nonnegligible influence on the retrieved mixing ratios at 740 K; therefore the apparent signature of denitrification at the topmost levels may be partially attributable to lower altitudes. Nevertheless, the MLS HNO_3 measurements shown here provide further evidence that denitrification can proceed in the absence of dehydration.

5. HNO_3 Measurements From EOS MLS

[38] A second-generation MLS experiment was launched as part of NASA's EOS Aura mission in July 2004. The capability of the EOS MLS instrument, which has a design lifetime of 5 years (versus 18 months for UARS MLS), is greatly enhanced over that of its predecessor. Three radiometers (at 190, 240, and 640 GHz) will measure HNO_3. Retrievals using simulated radiances indicate that, compared with the UARS MLS data shown here, EOS MLS HNO_3 measurements will have better vertical resolution (~3 km, versus ~6 km for UARS MLS in the lower stratosphere) over a larger vertical range (215–3.2 hPa versus 100–4.6 hPa) with similar precision (~1.5 ppbv over most of the profile). The horizontal resolution will also be better: ~200–300 km along track and ~3–9 km across track (versus ~400 km × 400 km for UARS MLS). The simulation results suggest that average biases are expected to be small at most latitudes and altitudes, with the overall accuracy ~10% from 147 to 4.6 hPa. Perhaps most importantly, EOS MLS will perform measurements with the instrument fields of view scanning the limb in the orbit plane to provide latitudinal coverage that extends from 82°N to 82°S on every orbit, affording continuous monitoring of the polar regions (no monthly gaps arising from yaw maneuvers as on UARS).

[39] The improved spatial/temporal coverage and resolution of the EOS MLS HNO_3 measurements will greatly facilitate many polar process studies. For example, continuous coverage of polar latitudes together with simultaneous, colocated, high-quality H_2O and temperature measurements will allow observation of complete PSC lifecycles, from formation through dissipation, as well as intraseasonal, interhemispheric, and interannual differences in PSC development and evolution. In addition to providing further insight into PSC formation mechanisms, the EOS MLS data set will also allow monitoring of the onset and extent of denitrification and dehydration in both hemispheres over multiple years. Comparison of the EOS MLS HNO_3 measurements with the composite/climatological fields established from UARS MLS HNO_3 will permit us to track any changes in PSC formation and denitrification (as well as the interannual variability in these processes) and assess their sensitivity to changes in stratospheric temperature and/or water vapor that may occur.

[40] **Acknowledgments.** We thank C. Randall for very helpful comments and the U.K. Met Office (especially R. Swinbank) for meteorological analyses. The anonymous reviewers are thanked for their contributions in improving this paper. Work at the Jet Propulsion Laboratory, California Institute of Technology, was done under contract with the National Aeronautics and Space Administration.

References

Andrews, D. G. (1989), Some comparisons between the middle atmosphere dynamics for the Southern and Northern Hemispheres, *Pure Appl. Geophys.*, *130*, 213–232.

Austin, J., R. R. Garcia, J. M. Russell, S. Solomon, and A. F. Tuck (1986), On the atmospheric photochemistry of nitric acid, *J. Geophys. Res.*, *91*, 5477–5485.

Barath, F. T., et al. (1993), The Upper Atmosphere Research Satellite Microwave Limb Sounder Instrument, *J. Geophys. Res.*, *98*, 10,751–10,762.

Bauman, J. J., P. B. Russell, M. A. Geller, and P. Hamill (2003), A stratospheric aerosol climatology from SAGE II and CLAES measurements: 2. Results and comparisons, 1984–1999, *J. Geophys. Res.*, *108*(D13), 4383, doi:10.1029/2002JD002993.

Bingham, G. E., D. K. Zhou, B. Y. Bartschi, G. P. Anderson, D. R. Smith, J. H. Chetwynd, and R. M. Nadile (1997), Cryogenic Infrared Radiance Instrumentation for Shuttle (CIRRIS 1A) Earth limb spectral measurements, calibration, and atmospheric O_3, HNO_3, CFC-12, and CFC-11 profile retrieval, *J. Geophys. Res.*, *102*, 3547–3558.

Bowman, K. P. (1993), Large-scale isentropic mixing properties of the Antarctic polar vortex from analyzed winds, *J. Geophys. Res.*, *98*, 23,013–23,027.

Brasseur, G., and C. Granier (1992), Mount Pinatubo aerosols, chlorofluorocarbons, and ozone depletion, *Science*, *257*, 1239–1242.

Butchart, N., and E. E. Remsberg (1986), The area of the stratospheric polar vortex as a diagnostic for tracer transport on an isentropic surface, *J. Atmos. Sci.*, *43*, 1319–1339.

Coy, L., E. R. Nash, and P. A. Newman (1997), Meteorology of the polar vortex: Spring 1997, *Geophys. Res. Lett.*, *24*, 2693–2696.

Danilin, M. Y., M. L. Santee, J. M. Rodriguez, M. K. W. Ko, J. L. Mergenthaler, J. B. Kumer, A. Tabazadeh, and N. Livesey (2000), Trajectory hunting: A case study of rapid chlorine activation in December 1992 as seen by UARS, *J. Geophys. Res.*, *105*, 4003–4018.

Danilin, M. Y., et al. (2002), Trajectory hunting as an effective technique to validate multiplatform measurements: Analysis of the MLS, HALOE, SAGE-II, ILAS, and POAM-II data in October–November 1996, *J. Geophys. Res.*, *107*(D20), 4420, doi:10.1029/2001JD002012.

David, S. J., F. J. Murcray, A. Goldman, C. P. Rinsland, and D. G. Murcray (1994), The effect of the Mt. Pinatubo aerosol on the HNO_3 column over Mauna Loa, Hawaii, *Geophys. Res. Lett.*, *21*, 1003–1006.

de Zafra, R. L., and S. P. Smyshlyaev (2001), On the formation of HNO_3 in the Antarctic mid to upper stratosphere in winter, *J. Geophys. Res.*, *106*, 23,115–23,125.

de Zafra, R. L., V. Chan, S. Crewell, C. Trimble, and J. M. Reeves (1997), Millimeter wave spectroscopic measurements over the South Pole: 3. The behavior of stratospheric nitric acid through polar fall, winter, and spring, *J. Geophys. Res.*, *102*, 1399–1410.

de Zafra, R. L., G. Muscari, and S. P. Smyshlyaev (2003), On the cryogenic removal of NO_y from the Antarctic polar stratosphere, *Ann. Geophys.*, *46*, 285–294.

Fischer, H., and H. Oelhaf (1996), Remote sensing of vertical profiles of atmospheric trace constituents with MIPAS limb-emission spectrometers, *Appl. Opt.*, *35*, 2787–2796.

Fromm, M. D., J. D. Lumpe, R. M. Bevilacqua, E. P. Shettle, J. Hornstein, S. T. Massie, and K. H. Fricke (1997), Observations of Antarctic polar stratospheric clouds by POAM II: 1994–1996, *J. Geophys. Res.*, *102*, 23,659–23,672.

Fromm, M. D., R. M. Bevilacqua, J. Hornstein, E. P. Shettle, K. Hoppel, and J. D. Lumpe (1999), An analysis of Polar Ozone and Aerosol Measurement POAM II Arctic stratospheric cloud observations, 1993–1996, *J. Geophys. Res.*, *104*, 24,341–24,357.

Gille, J. C., and J. M. Russell (1984), The Limb Infrared Monitor of the Stratosphere: Experiment description, performance, and results, *J. Geophys. Res.*, *89*, 5125–5140.

Gille, J. C., et al. (1984), Accuracy and precision of the nitric acid concentrations determined by the Limb Infrared Monitor of the Stratosphere experiment on Nimbus 7, *J. Geophys. Res.*, *89*, 5179–5190.

Gunson, M. R., et al. (1996), The Atmospheric Trace Molecule Spectroscopy (ATMOS) experiment: Deployment on the ATLAS Space Shuttle missions, *Geophys. Res. Lett.*, *23*, 2333–2336.

Hofmann, D. J., and S. Solomon (1989), Ozone destruction through heterogeneous chemistry following the eruption of El Chichòn, *J. Geophys. Res.*, *94*, 5029–5041.

Irie, H., et al. (2002), Validation of NO_2 and HNO_3 measurements from the Improved Limb Atmospheric Spectrometer (ILAS) with the version 5.20 retrieval algorithm, *J. Geophys. Res.*, *107*(D24), 8206, doi:10.1029/2001JD001304.

Irion, F., et al. (2002), Atmospheric Trace Molecule Spectroscopy (ATMOS) Experiment version 3 data retrievals, *Appl. Opt.*, *41*, 6968–6979.

Kawa, S. R., J. B. Kumer, A. R. Douglass, A. E. Roche, S. E. Smith, F. W. Taylor, and D. J. Allen (1995), Missing chemistry of reactive nitrogen in the upper stratospheric polar winter, *Geophys. Res. Lett.*, *22*, 2629–2632.

Knox, J. A. (1998), On converting potential temperature to altitude in the middle atmosphere, *Eos Trans. AGU*, *79*, 376.

Koike, M., N. B. Jones, W. A. Matthews, P. V. Johnston, R. L. McKenzie, D. Kinnison, and J. Rodriguez (1994), Impact of Pinatubo aerosols on the partitioning between NO_2 and HNO_3, *Geophys. Res. Lett.*, *21*, 597–600.

Koike, M., et al. (2000), A comparison of Arctic HNO_3 profiles measured by the Improved Limb Atmospheric Spectrometer and balloon-borne sensors, *J. Geophys. Res.*, *105*, 6761–6771.

Kumer, J. B., et al. (1996), Comparison of correlative data with HNO_3 version 7 from the CLAES instrument deployed on the NASA Upper Atmosphere Research Satellite, *J. Geophys. Res.*, *101*, 9621–9656.

Lee, A. M., H. K. Roscoe, A. E. Jones, P. H. Haynes, E. F. Shuckburgh, M. W. Morrey, and H. C. Pumphrey (2001), The impact of the mixing properties within the Antarctic stratospheric vortex on ozone loss in spring, *J. Geophys. Res.*, *106*, 3203–3211.

Livesey, N. J., W. G. Read, L. Froidevaux, J. W. Waters, M. L. Santee, H. C. Pumphrey, D. L. Wu, Z. Shippony, and R. F. Jarnot (2003), The UARS Microwave Limb Sounder version 5 data set: Theory, characterization, and validation, *J. Geophys. Res.*, *108*(D13), 4378, doi:10.1029/2002JD002273.

Manney, G. L., and R. W. Zurek (1993), Interhemispheric comparison of the development of the stratospheric polar vortex during fall: A 3-dimensional perspective for 1991–92, *Geophys. Res. Lett.*, *20*, 1275–1278.

Manney, G. L., R. W. Zurek, A. O'Neill, and R. Swinbank (1994), On the motion of air through the stratospheric polar vortex, *J. Atmos. Sci.*, *51*, 2973–2994.

Manney, G. L., H. A. Michelsen, M. L. Santee, M. R. Gunson, F. W. Irion, A. E. Roche, and N. J. Livesey (1999), Polar vortex dynamics during spring and fall diagnosed using trace gas observations from the Atmospheric Trace Molecule Spectroscopy instrument, *J. Geophys. Res.*, *104*, 18,841–18,866.

McDonald, M., R. L. de Zafra, and G. Muscari (2000), Millimeter wave spectroscopic measurements over the South Pole: 5. Morphology and evolution of HNO_3 vertical distribution, 1993 versus 1995, *J. Geophys. Res.*, *105*, 17,739–17,750.

Mills, M. J., A. O. Langford, T. J. O'Leary, K. Arpag, H. L. Miller, M. H. Proffitt, R. W. Sanders, and S. Solomon (1993), On the relationship between stratospheric aerosols and nitrogen dioxide, *Geophys. Res. Lett.*, *20*, 1187–1190.

Mills, M. J., O. B. Toon, and S. Solomon (1999), A 2D microphysical model of the polar stratospheric CN layer, *Geophys. Res. Lett.*, *26*, 1133–1136.

Murtagh, D., et al. (2002), An overview of the Odin atmospheric mission, *Can. J. Phys.*, *80*, 309–319.

Muscari, G., M. L. Santee, and R. L. de Zafra (2002), Intercomparison of stratospheric HNO_3 measurements over Antarctica: Ground-based millimeter-wave versus UARS/MLS version 5 retrievals, *J. Geophys. Res.*, *107*(D24), 4809, doi:10.1029/2002JD002546.

Nedoluha, G. E., R. M. Bevilacqua, K. W. Hoppel, M. Daehler, E. P. Shettle, J. H. Hornstein, M. D. Fromm, J. D. Lumpe, and J. E. Rosenfield (2000), POAM III measurements of dehydration in the Antarctic lower stratosphere, *Geophys. Res. Lett.*, *27*, 1683–1686.

Nedoluha, G. E., R. M. Bevilacqua, K. W. Hoppel, J. D. Lumpe, and H. Smit (2002), Polar Ozone and Aerosol Measurement III measurements of water vapor in the upper troposphere and lowermost stratosphere, *J. Geophys. Res.*, *107*(D10), 4103, doi:10.1029/2001JD000793.

Offermann, D., K.-U. Grossmann, P. Barthol, P. Knieling, M. Riese, and R. Trant (1999), Cryogenic Infrared Spectrometers and Telescopes for the Atmosphere (CRISTA) experiment and middle atmosphere variability, *J. Geophys. Res.*, *104*, 16,311–16,325.

O'Neill, A., and V. D. Pope (1990), The seasonal evolution of the extratropical stratosphere in the Southern and Northern Hemispheres: Systematic changes in potential vorticity and the non-conservative effects of radiation, in *Dynamics, Transport and Photochemistry in the Middle Atmosphere of the Southern Hemisphere*, edited by A. O'Neill, pp. 33–54, Kluwer Acad., Norwell, Mass.

Pawson, S., and B. Naujokat (1999), The cold winters of the middle 1990s in the northern lower stratosphere, *J. Geophys. Res.*, *104*, 14,209–14,222.

Poole, L. R., and M. C. Pitts (1994), Polar stratospheric cloud climatology based on Stratospheric Aerosol Measurement II observations from 1978 to 1989, *J. Geophys. Res.*, *99*, 13,083–13,089.

Randall, C. E., D. W. Rusch, R. M. Bevilacqua, K. W. Hoppel, and J. D. Lumpe (1998), Polar Ozone and Aerosol Measurement (POAM) II stratospheric NO_2, 1993–1996, *J. Geophys. Res.*, *103*, 28,361–28,371.

Randall, C. E., R. M. Bevilacqua, J. D. Lumpe, and K. W. Hoppel (2001), Validation of POAM III aerosols: Comparison to SAGE II and HALOE, *J. Geophys. Res.*, *106*, 27,525–27,536.

Randel, W. J., F. Wu, J. M. Russell, and J. W. Waters (1999), Space-time patterns of trends in stratospheric constituents derived from UARS measurements, *J. Geophys. Res.*, *104*, 3711–3727.

Read, W. G., L. Froidevaux, and J. W. Waters (1993), Microwave Limb Sounder (MLS) measurements of SO_2 from Mt. Pinatubo volcano, *Geophys. Res. Lett.*, *20*, 1299–1302.

Riese, M., R. Spang, P. Preusse, M. Ern, M. Jarisch, D. Offermann, and K. Grossmann (1999), Cryogenic Infrared Spectrometers and Telescopes for the Atmosphere (CRISTA) data processing and atmospheric temperature and trace gas retrieval, *J. Geophys. Res.*, *104*, 16,349–16,367.

Rinsland, C. P., et al. (1994), Heterogeneous conversion of N_2O_5 to HNO_3 in the post-Mount Pinatubo eruption stratosphere, *J. Geophys. Res.*, *99*, 8213–8219.

Rinsland, C. P., et al. (1999), Polar stratospheric descent of NO_y and CO and Arctic denitrification during winter 1992–1993, *J. Geophys. Res.*, *104*, 1847–1861.

Rinsland, C. P., D. K. Weisenstein, M. K. W. Ko, C. J. Scott, L. S. Chiou, E. Mahieu, R. Zander, and P. Demoulin (2003), Post-Mount Pinatubo eruption ground-based infrared stratospheric column measurements of HNO_3, NO, and NO_2 and their comparison with model calculations, *J. Geophys. Res.*, *108*(D15), 4437, doi:10.1029/2002JD002965.

Rodgers, C. D. (2000), *Inverse Methods for Atmospheric Sounding: Theory and Practice*, World Sci., River Edge, N. J.

Rosenlof, K. H., A. F. Tuck, K. K. Kelly, J. M. Russell, and M. P. McCormick (1997), Hemispheric asymmetries in water vapor and

inferences about transport in the lower stratosphere, *J. Geophys. Res.*, *102*, 13,213–13,234.

Russell, J. M., C. B. Farmer, C. P. Rinsland, R. Zander, L. Froidevaux, G. C. Toon, B. Gao, J. Shaw, and M. Gunson (1988), Measurements of odd nitrogen compounds in the stratosphere by the ATMOS experiment on Spacelab 3, *J. Geophys. Res.*, *93*, 1718–1736.

Santee, M. L., W. G. Read, J. W. Waters, L. Froidevaux, G. L. Manney, D. A. Flower, R. F. Jarnot, R. S. Harwood, and G. E. Peckham (1995), Interhemispheric differences in polar stratospheric HNO_3, H_2O, ClO, and O_3, *Science*, *267*, 849–852.

Santee, M. L., G. L. Manney, W. G. Read, L. Froidevaux, and J. W. Waters (1996), Polar vortex conditions during the 1995–96 Arctic winter: MLS ClO and HNO_3, *Geophys. Res. Lett.*, *23*, 3207–3210.

Santee, M. L., G. L. Manney, L. Froidevaux, R. W. Zurek, and J. W. Waters (1997), MLS observations of ClO and HNO_3 in the 1996–97 Arctic polar vortex, *Geophys. Res. Lett.*, *24*, 2713–2716.

Santee, M. L., G. L. Manney, L. Froidevaux, W. G. Read, and J. W. Waters (1999), Six years of UARS Microwave Limb Sounder HNO_3 observations: Seasonal, interhemispheric, and interannual variations in the lower stratosphere, *J. Geophys. Res.*, *104*, 8225–8246.

Schoeberl, M. R., L. R. Lait, P. A. Newman, and J. E. Rosenfield (1992), The structure of the polar vortex, *J. Geophys. Res.*, *97*, 7859–7882.

Siskind, D. E., J. T. Bacmeister, M. E. Summers, and J. M. Russell (1997), Two-dimensional model calculations of nitric oxide transport in the middle atmosphere and comparison with Halogen Occultation Experiment data, *J. Geophys. Res.*, *102*, 3527–3545.

Siskind, D. E., G. E. Nedoluha, C. E. Randall, M. Fromm, and J. M. Russell (2000), An assessment of Southern Hemisphere stratospheric NO_x enhancements due to transport from the upper atmosphere, *Geophys. Res. Lett.*, *27*, 329–332.

Slusser, J., et al. (1998), High-latitude stratospheric NO_2 and HNO_3 over Fairbanks (65°N) 1992–1994, *J. Geophys. Res.*, *103*, 1549–1554.

Solomon, S. (1999), Stratospheric ozone depletion: A review of concepts and history, *Rev. Geophys.*, *37*, 275–316.

Stone, E. M., A. Tabazadeh, E. Jensen, H. C. Pumphrey, M. L. Santee, and J. L. Mergenthaler (2001), Onset, extent, and duration of dehydration in the Southern Hemisphere polar vortex, *J. Geophys. Res.*, *106*, 22,979–22,989.

Swinbank, R., and A. O'Neill (1994), A stratosphere-troposphere data assimilation system, *Mon. Weather Rev.*, *122*, 686–702.

Tabazadeh, A., M. L. Santee, M. Y. Danilin, H. C. Pumphrey, P. A. Newman, P. J. Hamill, and J. L. Mergenthaler (2000), Quantifying denitrification and its effect on ozone recovery, *Science*, *288*, 1407–1411.

Taylor, F., J. Ballard, A. Dudhia, M. Goss-Custard, B. Kerridge, A. Lambert, M. Lopez-Valverde, C. Rodgers, and J. Remedios (1994), Stratospheric and mesospheric observations with ISAMS, *Adv. Space Res.*, *14*(9), 41–52.

Taylor, F., C. Rodgers, J. Remedios, R. Grainger, A. Lambert, M. LopezValverde, M. Goss-Custard, and J. Reburn (1995), Global atmospheric chemistry from satellites: Results from UARS/ISAMS, *Faraday Discuss.*, *100*, 353–369.

Thomason, L. W., L. R. Poole, and T. Deshler (1997), A global climatology of stratospheric aerosol surface area density derived from Stratospheric Aerosol and Gas Experiment II measurements: 1984–1994, *J. Geophys. Res.*, *102*, 8967–8976.

Toon, G. C., C. B. Farmer, L. L. Lowes, P. W. Schaper, J.-F. Blavier, and R. H. Norton (1989), Infrared aircraft measurements of stratospheric composition over Antarctica during September 1987, *J. Geophys. Res.*, *94*, 16,571–16,596.

Trepte, C. R., R. E. Veiga, and M. P. McCormick (1993), The poleward dispersal of Mount Pinatubo volcanic aerosol, *J. Geophys. Res.*, *98*, 18,563–18,573.

Waters, J. W. (1993), Microwave limb sounding, in *Atmospheric Remote Sensing by Microwave Radiometry*, edited by M. A. Janssen, chap. 8, pp. 383–496, John Wiley, Hoboken, N. J.

Waters, J. W., et al. (1999), The UARS and EOS Microwave Limb Sounder (MLS) experiments, *J. Atmos. Sci.*, *56*, 194–218.

Watterson, I. G., and A. F. Tuck (1989), A comparison of the longitudinal distributions of polar stratospheric clouds and temperatures for the 1987 Antarctic spring, *J. Geophys. Res.*, *94*, 16,511–16,525.

Waugh, D. W., and W. J. Randel (1999), Climatology of Arctic and Antarctic polar vortices using elliptical diagnostics, *J. Atmos. Sci.*, *56*, 1594–1613.

Waugh, D. W., W. J. Randel, S. Pawson, P. A. Newman, and E. R. Nash (1999), Persistence of the lower stratospheric polar vortices, *J. Geophys. Res.*, *104*, 27,191–27,201.

Webster, C. R., R. D. May, M. Allen, L. Jaegle, and M. P. McCormick (1994), Balloon profiles of stratospheric NO_2 and HNO_3 for testing the heterogeneous hydrolysis of N_2O_5 on sulfate aerosols, *Geophys. Res. Lett.*, *21*, 53–56.

World Meteorological Organization (2003), Scientific assessment of ozone depletion: 2002, *Rep. 47*, Global Ozone Res. and Monit. Proj., Geneva.

Zurek, R. W., G. L. Manney, A. J. Miller, M. E. Gelman, and R. M. Nagatani (1996), Interannual variability of the north polar vortex in the lower stratosphere during the UARS mission, *Geophys. Res. Lett.*, *23*, 289–292.

N. J. Livesey, W. G. Read, and M. L. Santee, Jet Propulsion Laboratory, Mail Stop 183-701, 4800 Oak Grove Drive, Pasadena, CA 91109, USA. (mls@mls.jpl.nasa.gov)

G. L. Manney, Department of Natural Sciences, New Mexico Highlands University, Las Vegas, NM 87701, USA.